NASA CR-134809
PSI TR-20

NASA

RADIANT ENERGY ABSORPTION STUDIES FOR LASER PROPULSION

by

G. E. Caledonia, P. K. S. Wu and A. N. Pirri

PHYSICAL SCIENCES INC.

prepared for

NATIONAL AERONAUTICS AND SPACE ADMINISTRATION
NASA Lewis Research Center

Contract NAS 3-18528

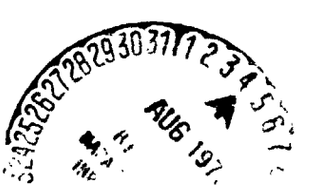

1 Report No.	2. Government Accession No.	3. Recipient's Catalog No.
NASA CR-134809		

4 Title and Subtitle	5. Report Date
RADIANT ENERGY ABSORPTION STUDIES FOR LASER PROPULSION	March 1975
	6. Performing Organization Code: 6K561
7. Author(s): G. E. Caledonia, P.K.S. Wu and A. N. Pirri	8. Performing Organization Report No: PSI TR-20
9. Performing Organization Name and Address: Physical Sciences Inc., 18 Lakeside Office Park, Wakefield, MA 01880	10. Work Unit No.
	11. Contract or Grant No: NAS 3-18528
12. Sponsoring Agency Name and Address: National Aeronautics and Space Administration, Lewis Research Center, Cleveland, Ohio 44135	13. Type of Report and Period Covered: Final Report, June 7, 1974 - Jan. 7, 1975
	14 Sponsoring Agency Code: 5331 500-318

15 Supplementary Notes

Project Monitor, Stephen M. Cohen, Laser and Energy Systems Branch, NASA Lewis Research Center, Cleveland, Ohio

16. Abstract

A study of the energy absorption mechanisms and fluid dynamic considerations for efficient conversion of high power laser radiation into a high velocity flow is presented. Although the contents of this study are applicable to the laser propulsion concept, they are not unique to this application and are useful for analysis of any system which requires the efficient conversion of laser energy to kinetic energy. The objectives are (1) to determine the most effective absorption mechanisms for converting laser radiation into translational energy, and (2) examine the requirements for transfer of the absorbed energy into a steady flow which is stable to disturbances in the absorption zone. The first part of the study consists of a review of inverse Bremsstrahlung, molecular and particulate absorption mechanicms. The second part of the study consists of steady flow and stability considerations for conversion of the laser power to a high velocity flow in a nozzle configuration. The quasi-one-dimensional flow through a nozzle is formulated under the assumptions of perfect gas, instantaneous conversion of absorbed laser energy to temperature (equilibrium flow) and an absorption coefficient proportional to density and temperature raised to arbitrary powers. For a specified nozzle configuration, predictions of Mach number, temperature, density and exhaust velocity are presented as a function of optical depth and the ratio of the laser power to inlet flow power. A "local" stability analysis is performed and a typical stability map of disturbance wavenumber versus nozzle position is presented. Neutral stability contours provide an indicator for proper design of nozzles with stable absorption zones.

17. Key Words (Suggested by Author(s))	18. Distribution Statement
Laser propulsion Radiant energy absorption Laser effects	Unclassified

19. Security Classif (of this report)	20 Security Classif (of this page)	21 No of Pages	22 Price*
Unclassified	Unclassified	71	

* For sale by the National Technical Information Service, Springfield, Virginia 22151

NASA CR-134809
PSI TR-20

RADIANT ENERGY ABSORPTION STUDIES FOR LASER PROPULSION

by

G. E. Caledonia, P. K. S. Wu and A. N. Pirri

PHYSICAL SCIENCES INC.

prepared for

NATIONAL AERONAUTICS AND SPACE ADMINISTRATION

NASA Lewis Research Center

Contract NAS 3-18528

FOREWORD

The research described in this report was performed for the Laser and Energy Systems Branch at the NASA-Lewis Research Center. The NASA Project Manager was Mr. Stephen M. Cohen.

The authors would like to acknowledge Dr. R. L. Taylor for his contributions to the large molecule absorption section (Sec. 3.3), and to M I. Scanzillo for her assistance in preparing and editing this report.

TABLE OF CONTENTS

SUMMARY

A study of the energy absorption mechanisms and fluid dynamic considerations for efficient conversion of high power laser radiation into a high velocity flow is presented. Although the contents of this study are applicable to the laser propulsion concept, they are not unique to this application and are useful for analysis of any system which requires the efficient conversion of laser energy to kinetic energy. The objectives are (1) to determine the most effective absorption mechanisms for converting laser radiation into translational energy, and (2) examine the requirements for transfer of the absorbed energy into a steady flow which is stable to disturbances in the absorption zone. The first part of the study consists of a review of inverse Bremsstrahlung, molecular and particulate absorption mechanisms.

Inverse Bremsstrahlung offers the advantage of spectral continuum absorption along with the rapid conversion of absorbed energy into translational modes. However, some mechanisms must be applied to provide an initial electron concentration, and until the gas becomes fully ionized, the absorption coefficient is strongly temperature dependent. The latter may induce unstable heating. A review of experimental and theoretical work in electron-neutral and electron-ion Bremsstrahlung is presented.

Molecular absorption offers the advantage of significant absorption at low temperatures plus the possible weak dependence of the absorption coefficient upon temperature. In general, however, molecular absorption requires coincidence between wavelengths of lasing and absorbing transitions, may "bleach" at large laser fluxes, requires additional techniques for converting vibrational energy to translational energy and may lose its efficiency for absorption via chemical reactions. It is proposed that the first and second of the above disadvantages of molecular absorption can be mitigated by high pressures, and high pressure molecular absorption is modeled. In addition, an analysis of a potential system for converting the absorbed energy into translation by using atomic species to vibrationally deactivate the absorbing molecule is presented.

Particulates offer the advantages of continuum absorption, rapid conversion of laser energy to translational energy and high conversion efficiency since only a small percentage of total absorbed energy remains in the particle. Modeling of the gas heating characteristics suggests that optimization occurs for very small particles at mass loadings of the order of 10^{-4} gms/cm^3. As the particles approach the boiling point other mechanisms such as molecular absorption and Bremsstrahlung can become the dominant absorption mechanisms, and vaporization and radiative losses from the particles may decrease their absorption efficiency.

The second part of the study consists of steady flow and stability considerations for conversion of the laser power to a high velocity flow in a nozzle configuration. The quasi-one-dimensional flow through a nozzle is formulated under the assumptions of perfect gas, instantaneous conversion of absorbed laser energy to temperature (equilibrium flow) and an absorption coefficient proportional to density and temperature raised to arbitrary powers. For a specified nozzle configuration, predictions of Mach number, temperature, density and exhaust velocity are presented as a function of optical depth and the ratio of the laser power to inlet flow power. A "local" stability analysis is performed and a typical stability map of disturbance wavenumber versus nozzle position is presented. Neutral stability contours provide an indicator for proper design of nozzles with stable absorption zones.

1. INTRODUCTION

The success of any system designed to convert high power laser radiation into directed kinetic energy depends upon the ability of the system to perform this conversion efficiently. Neither the existing research on the use of remotely stationed lasers to power a rocket engine[1-3] nor the work of Hertzberg et al[4] on the thermodynamics of a photon engine have a priori addressed the fundamental issue of the most efficient process by which a flowing gas can absorb laser radiation and convert it to useful work. The research in laser propulsion[1,2] relied upon the creation of electrons via breakdown to initiate absorption by inverse Bremsstrahlung and subsequent conversion of the heated gas into kinetic energy to obtain high specific impulse. However, the experiments[2] illustrated a posteriori that (for solid propellants) without some tailoring of the propellant composition, the conversion process yields the initiation of absorption waves in the gas.[2] The result was unsteady flow behavior and low power conversion efficiency. No attempts were made to determine whether other absorbers (e.g. molecular or particulate) would provide a stable and efficient method for converting laser radiation into directed kinetic energy.

What is necessary for any application which requires the conversion of coherent laser radiation into flow work are answers to the following questions:

(1) What are the best absorbers to make this conversion from radiation to translational energy most efficient?

(2) Is the absorption of laser radiation by a flowing gas a steady process where the gas enters the absorbing region in one state and exits in another? In addition, upon leaving the absorption zone, has the absorbed energy been stored in an excited molecular state to be converted to translational energy downstream?

(3) Is the conversion process stable to disturbances in the absorbing region?

This report is aimed at providing the first step toward answering the above questions. The report is essentially divided into two major parts. The next three sections are devoted to a review of absorption mechanisms to

convert laser energy to translational energy. Section 2 consists of a review of inverse Bremsstrahlung absorption. Section 3 discusses the properties of molecular absorption and presents an analysis of a proposed molecular absorption system at high pressure. Section 4 is devoted to a discussion of radiative absorption via particulates. The last section describes the second part of our program and presents fluid dynamic considerations for converting the absorbed laser energy to a high velocity flow. Steady solutions for the quasi-one-dimensional nozzle flow of a coherent radiation absorbing gas are presented. In addition, a stability analysis is described and applied to the nozzle flow to determine under what conditions the conversion process is stable to disturbances in the absorbing region.

2. INVERSE BREMSSTRAHLUNG

2.1 INTRODUCTION

When a free electron is in a close encounter with an atom or molecule it will undergo an acceleration caused by the potential field between the collision pair. In the case of collision with an ion the dynamics of the collision is dominated by the long range coulombic (or screened coulombic) field whereas in the collision with a neutral species the resulting induced fields, dipole or higher, are short range in nature. It is well known from classical electrodynamics that an accelerating electron radiates continuously, and in the process loses part of its kinetic energy, thus, slowing down. For this reason the resulting radiation is called Bremsstrahlung (braking radiation) and the reverse absorption process is termed inverse Bremsstrahlung. The radiation resulting from electron-ion collisions is often called Kramers' radiation while that resulting from electron-neutral collisions is termed neutral Bremsstrahlung.

Bremmstrahlung radiation is of interest in many areas including astrophysical applications, laser heating of plasmas, and in the prediction of the infrared radiation from heated gases and has received considerable theoretical study. The interest of this work is in the prediction of the infrared inverse Bremsstrahlung absorption coefficient for light gases, such as Hydrogen or Helium, at temperatures less than 10,000°K. Recent[5, 6] detailed predictions and measurements of the absorption coefficients for these gases have been performed at temperatures above 10,000°K. In this instance the comparison between theory[6] and experiment[7] was excellent. Unfortunately, at lower temperatures, where the neutral Bremsstrahlung process dominates, there do not seem to be any experimental measurements for H and He and theoretical estimates must be relied upon.

Although a definitive review is not justified under the present effort, a general discussion of the theoretical work on Kramers radiation and neutral Bremsstrahlung will be given below. Perhaps the most detailed discussion of the semi-classical treatment of Kramers radiation and the related free bound processes may be found in the Handuch d. Physik article by Finkelnburg and Peters.[8] Both Biberman and Norman[9] and Johnston[10] have presented surveys of the theoretical work performed in this area up to 1967. A number of more recent efforts are referenced in Ref. 5 and 6. The available measurements of neutral Bremsstrahlung cross-sections at infrared wavelengths are limited and to our knowledge have never been reviewed.

In this section the data base will be compared with theoretical predictions wherever possible.

2.2 KRAMERS RADIATION (ELECTRON-ION BREMSSTRAHLUNG)

A free electron by itself cannot absorb a photon and conserve both momentum and energy, however, if a third body is available to pick up the recoil momentum, the process is allowed. Kramers[11] was the first to develop a semi-classical model for this phenomenon for the case of an electron interacting with a hydrogenic ion in a pure coulomb field. His result for the absorption coefficient was

$$k_\nu = \sigma_{ei}\, n_e\, n_i\, (e^{+h\nu/kT} - 1),\ cm^{-1} \qquad (2.1)$$

where σ_{ei} is the electron-ion absorption cross-section, n_e and n_i, the electron and ion densities respectively, and ν the frequency of the laser. The bracketed term represents a product of two distinct effects. The first being a factor of $(1-e^{-h\nu/kT})$ which is a correction term for stimulated emission, and the second, a factor of $e^{h\nu/kT}$, which includes the effect of bound-free absorption from high lying electronic states. This latter term was derived[12] under the assumption that the electron and electronic temperatures are in equilibrium and should not be used indiscriminately. In anv event this latter term is unimportant for $h\nu/kT \ll 1$.

The quantity σ_{ei} is given by

$$\sigma_{ei} = \frac{4}{3}\left(\frac{2\pi}{3\,m\,k\,T}\right)^{1/2} \frac{Z^2\, e^6}{h\,c\,m\,\nu^3},\ cm^5 \qquad (2.2)$$

$$= \frac{3.7 \times 10^8\, Z^2}{T^{1/2}\, \nu^3}$$

where Z^2 is the effective nuclear charge, e is the unit charge, m is the electron mass, k is Boltzmanns constant and h is Planks constant. The basic assumptions in this derivation are a pure coulomb potential field (hydrogenic ions) and an electron velocity distribution defined by a Maxwellian distribution at the temperature T.

The quantum mechanical derivation was first considered by Gaunt.[13] The results are complex but may be evaluated accurately for the case of a hydrogenic ion. The quantum mechanical solution is generally written in terms of the classical solution, Eq. (2.2), multiplied by a correction factor g (λ, T), called the Gaunt Factor. There is no simple formulation for the Gaunt Factor, however, it has been tabulated extensively by Karzas and Latter[14] among others. For our conditions of interest, $0.1 \lesssim h\nu \lesssim 1$ ev, $1000 \leq T \leq 10,000^{\circ}K$, the Gaunt Factor is $\sim 1.3 \pm 0.2$.

The quantum mechanical prediction for ions other than hydrogenic is considerably more complicated because of screening effects as well as distortion of the electronic cloud. However, the long range coulomb field can dominate the momentum absorption process for low energy photons resulting in cross sections similar to that for hydrogenic ions. This point is discussed by Johnston,[10] and small first order corrections for species such as He have been calculated by Peach.[15]

2.3 NEUTRAL BREMSSTRAHLUNG

2.3.1 Theory

Free-free absorption in the presence of a neutral atom will dominate Kramers radiation when the fractional concentration of ions is $\lesssim 10^{-2}$. The basic complication in evaluating the cross sections for this process is in defining the interaction potential between the electron and the neutral species. This is particularly complicated in the case of an n electron atom or molecule and generally an effective spherically symmetric potential is assumed.

Following Geltman[16] the differential cross section for the absorption of a photon of energy $h\nu$ by an electron of initial wave vector k_i resulting in the final wave vector k_f is given by[16]

$$\frac{d\sigma_{en}}{d\Omega_f} = \frac{e^2 m \nu k_f}{\hbar^2 c} \left| < f \left| \hat{\epsilon} \cdot \vec{r} \right| i > \right|^2 \qquad (2.3)$$

where $\hat{\epsilon}$ is the electric field polarization unit vector and $|i>$ and $|f>$ are the contimuum states $\psi^{+}_{k_i}, \psi^{-}_{k_f}$. The partial wave expansion of the continuum states is[16]

$$\psi^{\perp}_{k}(r) \sum_{\ell=0}^{\infty} i^{\ell} (2\ell+1) e^{\perp i \eta_{\ell}} \frac{u_{\ell}(k,r)}{kr} P_{\ell}(\hat{k} \cdot \vec{r}) \qquad (2.4)$$

where n_ℓ is the scattering phase shift and $u_\ell (k \cdot r)$ is the radial wave function defined by[16]

$$\left[d^2/dr^2 - \frac{\ell (\ell + 1)}{r^2} - U(r) + k^2 \right] u_\ell = 0 \qquad (2.5)$$

where U (r) is the potential function defining the electron-neutral interaction. The overall absorption cross section, Q_{en}, is determined by integrating Eq. (2.3) over all incident and final electron directions and then performing a Maxwell average. The resulting absorption coefficient is given by[16]

$$k_{\nu,en} = Q_{en}\ n_e\ n_N (1 - e^{-h\nu/kT}),\ cm^{-1} \qquad (2.6)$$

where n_e and n_N are the electron and neutral densities respectively and the bracketed term is a correction for stimulated emission.

Early evaluations[17, 18] of expression (2.3) were carried out to first order, s wave only, and the resulting terms could be related to the elastic scattering or momentum transfer cross sections, thus eliminating the need for specification of the interaction potential. More recent calculations (refs. 16, 19, 20 among many others) included exchange effects ($\ell > 0$) with a variety of potential functions for more accurate predictions. Much of this work is discussed in Johnstons[10] review. Available predictions for the species H, H_2 and He are discussed below.

2.3.1.1 Hydrogen Atoms

The prediction of the neutral Bremsstrahlung cross-section for hydrogen atoms has received considerable theoretical analysis over the years because of its importance in astrophysics. Detailed predictions, including exchange effects have been presented by John[19], Geltman[20], Doughty and Fraser[21] and Stilley and Callaway.[22] The results of these various treatments are substantially in agreement with the results generally being presented in tabular and/or graphical form.

The first relatively accurate, (in comparison to detailed numerical calculations), analytical expression for the H atom neutral Bremsstrahlung cross-section was presented by Dalgarno and Lane.[23] In this analysis the right side of (Eq. 2.3) was expanded to first order in terms of the zero-order elastic scattering cross section q_o (E), where E is the electron energy. The latter quantity was expanded at low energies by use of effective range theory[24] with the result

$$q_o(E) = 4\pi (D_1 + D_2 E^{1/2} + D_3 E \ell n(E) + D_4 E + D_5 E^{3/2}) a_o^2$$

where a_o is the Bohr radius and the quantities D_i may be related to molecular parameters. Their resulting expression for the absorption cross section was

$$Q_{en} = 4.51 \times 10^{-34} T^{-3/2} (1 - e^{-a})^{-1} \left[D_1 I_1(a) + b^{1/2} D_2 I_2(a) + b D_3 I_3(a) + b D_3 \frac{3}{a} I_1(a) \ell n(b) + b D_4 \frac{3}{a} I_1(a) + b^{3/2} D_5 I_4(a) + \ldots \right] \qquad (2.7)$$

where $a = h\nu/kT$, $b = 1.2395/\lambda$ (μm) and the quantities $I_i(a)$ are integrals which were tabulated vs a. These latter quantities are reproduced in Table 2.1.

Dalgarno and Lane applied Eq. (2.7) to a number of atoms and molecules. For the case of H atoms the relevant parameters are $D_1 = 11.24$, $D_2 = 7.2$, $D_3 = 4.959$, $D_4 = -11.58$ and $D_5 = -0.4023$. Eq. (2.7) was shown to provide good agreement with the more detailed calculations of Geltman.[20] Dalgarno and Lane[23] suggest that for the case of H atoms relationship (2.7) should be accurate for values of λ and T such that $(a + 2)\, T < 30{,}000^{\circ}K$.

Very recently Stallcop[25] has developed a very simple analytic expression for the H atom neutral Bremsstrahlung cross section valid in the limit where $h\nu/kT$ is small. In this work the absorption cross section is again defined in terms of the elastic scattering cross-section, and after a number of mathematical approximations it is shown that

$$Q_{en_H} \approx 2.96 \times 10^{-45} T (1 - e^{-h\nu/kT})^{-1} (E_H/h\nu)^2 \cdot \exp(-\xi(k_T))/k_T \ , \ cm^5 \qquad (2.8)$$

where $k_T = (kT/E_H)^{1/2}$, E_H is the ionization potential for hydrogen atoms and

TABLE 2.1

PARAMETERS FOR PREDICTION OF NEUTRAL BREMSSTRAHLUNG CROSS SECTIONS (DALGARNO & LANE, 1966)

a	$I_1(a)$	$I_2(a)$	$I_3(a)$	$I_4(a)$
0.02	1.000×10^{4}	1.175×10^{5}	7.752×10^{6}	2.056×10^{7}
0.04	2.500×10^{3}	2.077×10^{4}	8.390×10^{5}	1.817×10^{6}
0.06	1.111×10^{3}	7.537×10^{3}	2.261×10^{5}	4.397×10^{5}
0.08	6.249×10^{2}	3.671×10^{3}	8.863×10^{4}	1.606×10^{5}
0.10	3.999×10^{2}	2.101×10^{3}	4.270×10^{4}	7.356×10^{4}
0.15	1.777×10^{2}	7.622×10^{2}	1.121×10^{4}	1.780×10^{4}
0.20	9.992×10^{1}	3.711×10^{2}	4.297×10^{3}	6.501×10^{3}
0.30	4.437×10^{1}	1.345×10^{2}	1.093×10^{3}	1.572×10^{3}
0.40	2.492×10^{1}	6.536×10^{1}	4.069×10^{2}	5.743×10^{2}
0.50	1.592×10^{1}	3.732×10^{1}	1.869×10^{2}	2.629×10^{2}
0.60	1.104×10^{1}	2.359×10^{1}	9.805×10^{1}	1.388×10^{2}
0.70	8.092	1.599×10^{1}	5.637×10^{1}	8.091×10^{1}
0.80	6.181	1.141×10^{1}	3.466×10^{1}	5.068×10^{1}
0.90	4.871	8.470	2.243×10^{1}	3.354×10^{1}
1.00	3.935	6.483	1.511×10^{1}	2.319×10^{1}
1.50	1.692	2.301	3.091	5.601
2.00	9.550×10^{-1}	1.096	9.088×10^{-1}	2.047
2.50	6.032×10^{-1}	6.141×10^{-1}	3.167×10^{-1}	9.404×10^{-1}

$$\xi(k_T) \approx 4.862\ k_T\ (1 - 0.2096\ k_T + 0.0170\ k_T^2 - 0.00968\ k_T^3) \qquad (2.9)$$

valid for $h\nu/k_T \lesssim 1$, $0.1 \lesssim k_T \lesssim 1$.

Stallcop has shown that this simple relationship is in good agreement with more detailed predictions.[19-22] Note that relationship (2.8) is valid at considerably higher temperatures than the expression of Dalgarno and Lane[23], Eq. (2.7), although the latter is to be preferred at the higher values of $h\nu/kT$. Absorption cross sections for H atoms, as determined from Eq. (2.8) are shown in Fig. 2.1 vs. temperature for wavelengths of 5 and 10 μm. The cross sections scale as the square of wavelength and approximately linearly with temperature over this temperature range.

2.3.1.2 Hydrogen Molecules

The neutral Bremsstrahlung absorption cross section for H_2 can be of considerable importance at low temperatures. For example, at a pressure of 10 atm the equilibrium concentration of H_2 will be greater than that of H at temperatures below 4100°K. Unfortunately, little theoretical effort has been directed towards the prediction of this cross section.

Although Dalgarno and Lanes'[23] analysis is strictly only appropriate for atoms, it has been applied to the Hydrogen molecule under the assumption that the low energy elastic scattering of an electron by a molecule is dominated by the spherically symmetric component of the molecular potential field. From Ref. 23 the relevant parameters to be used with Eq. (2.7) are $D_1 = 1.6456$, $D_2 = 5.8492$, $D_3 = 0.86147$, $D_4 = -2.6502$, $D_5 = 0.0$. The relationship is expected to be reliable for wavelength and temperature such that $(a + 2)\ T \lesssim 10{,}000°K$.

The only other prediction for H_2 appears to be that of Somerville.[26] His analysis is similar to Dalgarno and Lanes' with a slightly different approximation for $q_o(E)$. The latter work[23] is preferred. However, given the lack of experimental data it is difficult to determine its reliability.

2.3.1.3 Helium

The most recent predictions for He have been performed by Geltman[16] who used a full partial wave analysis, Eqs. (2.3) - (2.5), with model potentials that include a polarizability term. These predictions are

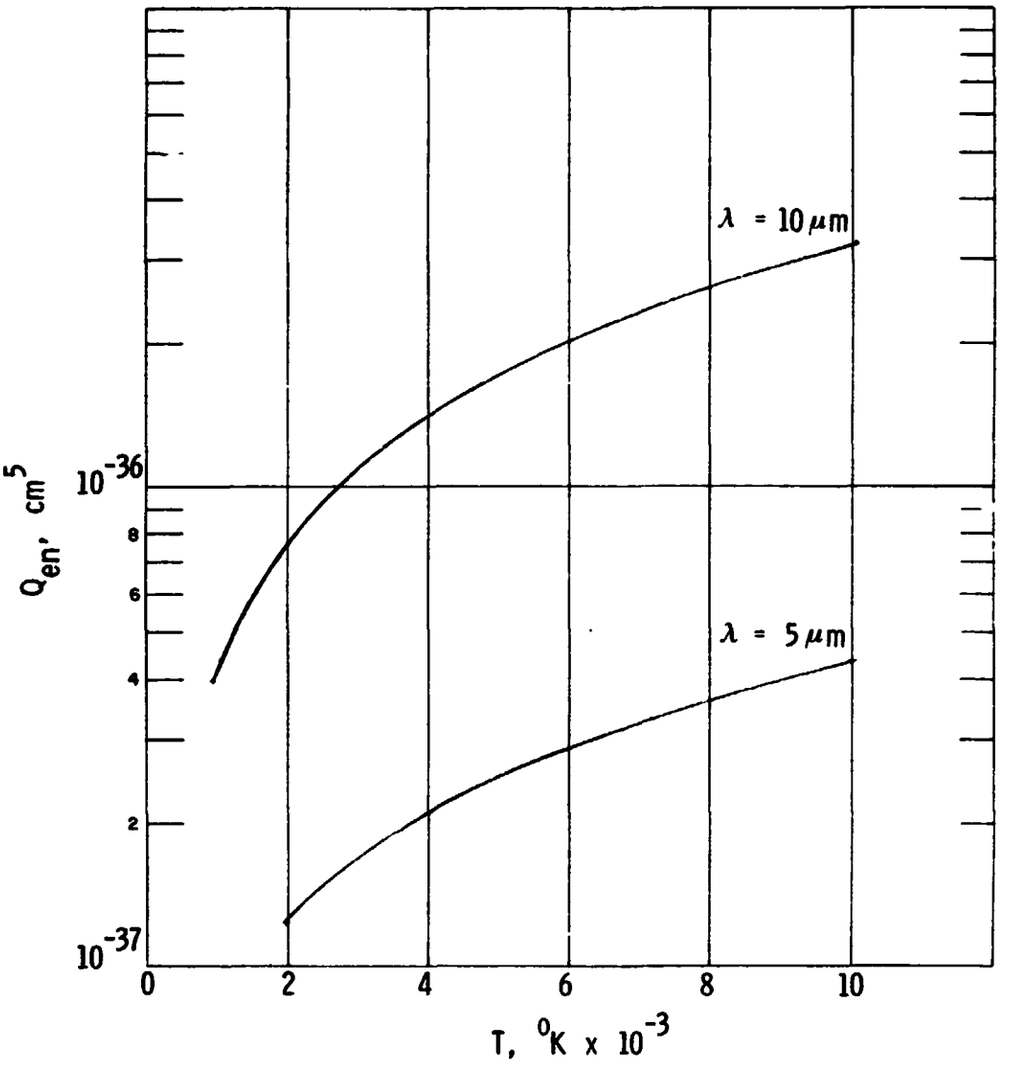

Fig. 2.1 Predicted Hydrogen Atom Neutral Bremsstrahlung Absorption Cross-Section vs. Temperature for λ = 5, 10 μm.

in good agreement with earlier work by McDowell et al[27] and are estimated by Geltman to be accurate to within 30%.

Predictions of the neutral Bremsstrahlung cross sections for He are tabulated in Ref. 16 over the wavelength range of 0.5 - 20 μm and temperature range from 500 - 20,000°K. Representative values at λ = 2.0, 5.0 and 10.00 μm are plotted vs temperature in Fig. 2.2. In this wavelength/temperature range the cross section scales approximately with the cube of wavelength and linearly with temperature. The cross sections are roughly a factor of 3 lower than those predicted for H atoms.

Theoretical predictions for a number of other atoms and molecules are also available. These include the rare gases,[16,23] heated air species,[16, 23, 27-29] and more recently the alkali atoms[30-32]. The work in this area is voluminous, the above references being representative rather than inclusive, and will not be reviewed here.

2.3.2 Comparison Between Theory and Experiment

There does not appear to be any experimental measurements of the cross-sections for infrared neutral Bremsstrahlung with H, He, H_2. There are a limited number of measurements for rare gas and air species and these are listed in Table 2.2 along with theoretical predictions taken from Refs. 16 and 28. There is minimal overlap between the conditions of the various measurements. However, where there is such overlap, the measurements are in agreement with the exception of the cross section for neon. What is remarkable is that in the infrared, experimental measurements for all gases shown are consistantly higher than the theoretical predictions, typically by a factor of two to four.

It is hard to rationalize this large difference between theory and experiment even though the experiments involved are admittedly complex. It would appear that considerable more effort, both experimental and theoretical, must be extended in this area before low temperature neutral Bremsstrahlung absorption cross sections may be predicted with a high degree of certainty. It should be emphasized, however, that the theoretical efforts are most appropriate to the hydrogen atom.

2.3.3 Example - Low Temperature Seeded Hydrogen Plasma

It is worthwhile to briefly discuss the dominant absorption process for a specific configuration. Equilibrium species concentrations[39] for pure hydrogen at 10 atm total pressure are shown in Fig. 2.3. Note that at the highest temperature shown (10,000°K) the equilibrium ion mole fraction

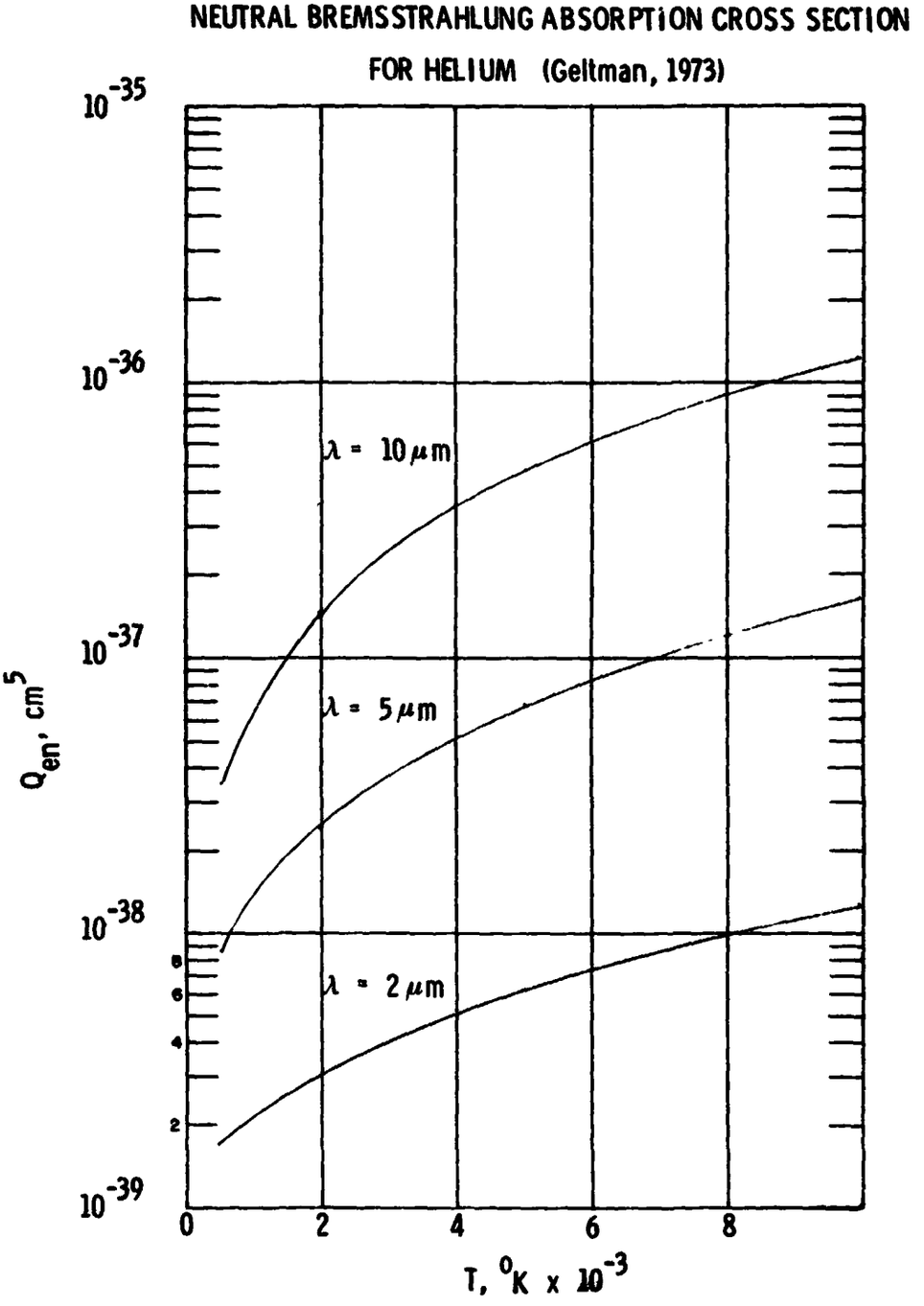

Fig. 2.2 Predicted Helium Atom Neutral Bremsstrahlung Absorption Cross-Section vs. Temperature for λ = 2., 5., 10. μm. Predictions taken from Ref. 16.

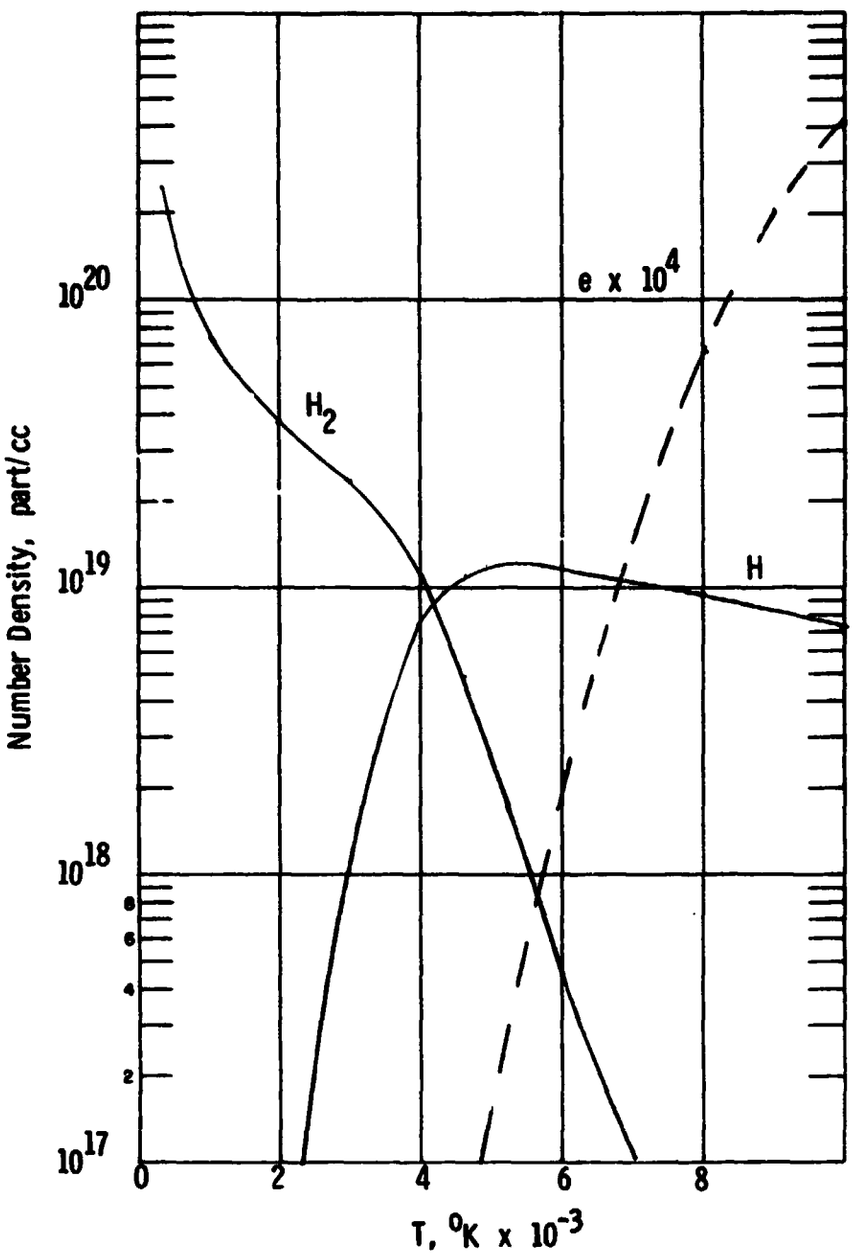

Fig. 2.3 Hydrogen Equilibrium Species Concentration vs. Temperature. P = 10 atm.

TABLE 2.2

COMPARISON OF EXPERIMENTAL MEASUREMENTS AND THEORETICAL PREDICTION FOR NEUTRAL BREMSSTRAHLUNG CROSS SECTIONS

Gas	T (^{o}K)	λ(μm)	Q_{en} (exp) cm^5	Q_{en} (theory) cm^5
He	5000	0.5	5.5×10^{-40}(a)	3.2×10^{-40}(g)
Ar	5000	0.5	1.8×10^{-40}(a)	1.8×10^{-40}(g)
	9700	3.1	1.0×10^{-37}(b) 7.5×10^{-38}(c)	2.5×10^{-38}(g)
		5.0	3.6×10^{-37}(b)	1.0×10^{-37}(g)
Ne	12,600	3.1	1.9×10^{-38}(b) 6.9×10^{-38}(c)	1.8×10^{-38}(g)
		5.0	7.2×10^{-38}(b)	7.2×10^{-38}(g)
		9.85	7.8×10^{-37}(c)	5.2×10^{-37}(g)
Xe	8200	2	3×10^{-38}(b)	1.5×10^{-38}(g)
		3.5	9.6×10^{-38}(b)	6.5×10^{-38}(g)
		5	2.0×10^{-37}(b)	1.7×10^{-37}(g)

TABLE 2.2 (cont.)

N	9175	2.	3.2×10^{-38}(d) 6.4×10^{-38}(e)	8.9×10^{-39}(g) 6.9×10^{-39}(h)
		3.5	$1.3 \cdot 10^{-37}$(d) $2.6 \cdot 10^{-37}$(e)	4.0×10^{-38}(g) 3.1×10^{-38}(h)
		5.0	3.0×10^{-37}(d)	1.1×10^{-37}(g) 9.8×10^{-38}(h)
O	5000	2.0	2.4×10^{-38}(f)	2.7×10^{-39}(g) 2.5×10^{-39}(h)
		5.0	2.6×10^{-37}(f)	2.9×10^{-38}(g) 3.6×10^{-38}(h)
	9700	3.1	7.6×10^{-38}(d) 7.8×10^{-38}(c)	2.3×10^{-38}(g) 1.0×10^{-38}(h)
		5.0	2.6×10^{-37}(d)	8.5×10^{-38}(g) 3.6×10^{-38}(h)
		9.85	3.0×10^{-36}(c)	1.0×10^{-36}(g)

TABLE 2.2 (cont.)

N2	8350	2.0	3.8×10^{-38}(d)	1.4×10^{-38}(h)
		3.5	1.3×10^{-37}(d)	7.0×10^{-38}(h)
		5.0	3.0×10^{-37}(d)	2.0×10^{-37}(h)
O2	5000	2.0	9.6×10^{-38}(f)	3.2×10^{-39}(h)
		5.0	1.0×10^{-36}(f)	3.7×10^{-38}(h)

a = ref. 33, b = ref. 34, c = ref. 35, d = ref. 36, e = ref. 37,
f = ref. 38, g = ref. 16 h = ref. 28

is 5.7×10^{-3}. It can readily be shown from a comparison of Eq. (2.2) to the neutral Bremsstrahlung cross sections shown in Fig. 2.1 that neutral Bremsstrahlung will dominate ionic for ion mole fractions $\leq 10^{-2}$. Thus, over the full temperature of Fig. 2.3 neutral Bremsstrahlung will be the dominant continuous absorption process. Even if a seed, such as Cs, were introduced a concentration of more than 2×10^{-2} in the cold gas would be required before ionic Bremsstrahlung would dominate. This large a concentration of Cs would produce the undesirable result of increasing the average molecular weight of the cold gas from 2 to 4.7 gms/mole.

Thus, it would appear that even for a seeded system, neutral Bremsstrahlung would provide the dominant continuous absorption mechanism below 10,000°K with collisions with the hydrogen molecule dominating below 4000°K. The remaining question is whether there will be any contributions to the total absorption coefficient from line absorption (i.e. bound-bound transitions). Very recently the infrared emission spectra of cesium contaminated air was measured[40] at a temperature of 3300°K under conditions where only 10% of the Cs was ionized. This measurement is shown in Fig. 2.4 with identification of the prominent Cs lines. The monochromator resolution is ~ 0.2 μm over this wavelength range. The Bremsstrahlung prediction is a semi-empirical extrapolation from the measurements of Taylor and Caledonia.[36] As can be seen there are several prominent Cs lines which could enhance the total absorption coefficient, although not at CO_2 laser wavelengths.

Hyman and vonRosenberg[40] have demonstrated an interesting feature concerning the spectral positioning of these atomic lines. This is that since infrared lines involve pairs of levels with high principal quantum numbers the spectrum will be fairly hydrogenic with the exception of a relatively small number of lines characteristic of the atom of interest. These hydrogenic lines typically involve states with the same principal quantum number n (unallowed transitions in hydrogen) or at most involve a change in n of unity. Hyman and vonRosenberg point out that the line positions of these transitions, which will occur in most atomic gases, may be specified by the relationship

$$\lambda\ (\mu m) = 0.0911\ \frac{n^2\ (n-1)^2}{2n-1} \quad (n \geq 5) \qquad (2.10)$$

and, thus, the first few lines will appear at 4.05, 7.46, 12.36 and 19.05 μm. The lowest of these lines would explain the ubiquitous 4 μm line which has been observed in a number of gases (see for instance the data in Refs. 34, 36). Note that prominent lines at these wavelengths are observed in the Cs spectrum shown in Fig. 2.4.

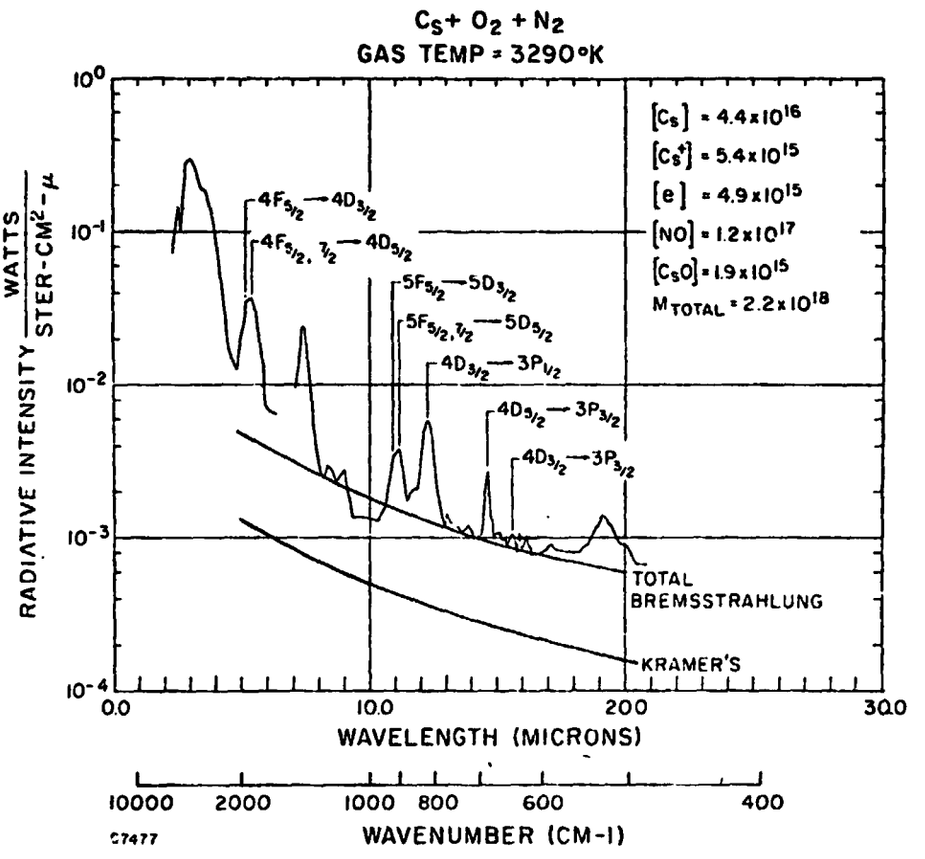

Fig. 2.4 Infrared Emission Spectrum of a Cs-Air Mixture. Line Identification corresponds to Cs Atomic Transitions. Conditions as shown. Taken from Ref. 40.

The prediction of the absorption coefficients for such bound-bound transitions is beyond the scope of the present work. It should be stressed that as the temperature is raised the Cs will become completely ionized in which case bound-bound transitions of the bath gas would be dominant.

2.4 SUMMARY

Theoretical predictions for the cross sections of inverse ionic and neutral Bremsstrahlung absorption have been reviewed. For the most part the discussion has been limited to the prediction of the infrared absorption cross sections for light gases, such as H, H_2 and He, at temperatures below 10,000°K. Although there is no data available for H, H_2 and He the measured infrared cross sections for other gases are typically a factor of two to four higher than theoretical predictions.

The particular case of a seeded hydrogen plasma has been discussed. Under equilibrium conditions the dominant continuous absorption process will be neutral Bremsstrahlung at temperatures below 10,000°K and seed levels $\lesssim$ 2%. Hydrogen molecules will be the dominant collision partner below 4000K and hydrogen atoms above. At the lower temperatures bound-bound transitions could provide the dominant absorption process at specific wavelengths. The Bremsstrahlung absorption coefficient is linearly proportional to electron density and thus, even in the presence of a seed will decrease exponentially with decreasing temperature at temperatures below 2500-3000°K.

3. MOLECULAR ABSORPTION

3.1 INTRODUCTION

As mentioned in the previous section, a basic disadvantage in using inverse Bremsstrahlung for laser gas heating is that under equilibrium conditions the Bremsstrahlung absorption coefficient decreases exponentially with decreasing temperature at low temperatures ($T \lesssim 3000^{\circ}K$ in the case of Cs, which has the lowest ionization potential of all the elements) and is negligibly small at room temperature. An alternate absorption mechanism which can be as (or more) effective in a cold gas as in a heated one is direct absorption by the vibration/rotation (V/R) bands of a seed molecule. This mechanism however does have a number of disadvantages not encountered in inverse Bremsstrahlung.

1) A given molecule will have a finite number of absorbing transitions which will occur over a limited wavelength range;

2) The absorbed energy is deposited in the vibrational rather than translational modes of the molecule and efficient kinetic mechanisms are required to convert the absorbed energy into heat. In particular, when the upper state of an absorbing transition is populated more rapidly than it can be de-activated, gas "bleaching" can occur;

3) As the gas temperature increases undesirable chemical phenomena, such as dissociation, can degrade the absorption process.

This last point is particularly important for larger molecules. For example, SF_6, which is an efficient absorber of CO_2 laser radiation, will be significantly dissociated at temperatures above $\sim 1700^{\circ}K$. Even a relatively stable triatomic such as CO_2 will dissociate at temperatures above $\sim 2500^{\circ}K$. Generally speaking, only diatomic molecules with large dissociation energies can provide significant laser gas heating with minimal chemical effects. As will be discussed below, the first two disadvantages may be minimized by performing the absorption in a high pressure system. Because of the complications introduced by chemical effects, the major portion of the discussion below will be limited to absorption by diatomic molecules. However, much of what is said will also hold true for larger molecules.

3.2 DIATOMIC ABSORPTION

The pressure broadened absorption coefficient for a given V/R transition with vibrational levels $v - 1 \rightarrow v$ and rotational levels $J \rightarrow J \pm 1$ is defined by

$$\alpha_{v-1,J,\Delta J}(\nu),\ \mathrm{cm}^{-1} = \frac{\lambda^2 \, A_{v-1,J,\Delta J}^{v,v-1,J,\Delta J}}{4\pi^2 \, c \, \Delta\nu_L} \left(N_{v-1,J} - \frac{g_{v-1,J}}{g_{v,J\pm1}} N_{v,J\pm1} \right) \left[4 \left(\frac{\nu - \nu_{v,J,\Delta J}}{\Delta\nu_L} \right) + 1 \right]^{-1} \tag{3.1}$$

where ν is wavenumber, c the speed of light, λ wavelength, A the Einstein coefficient of the transition, N the populations of the upper and lower states, g the degeneracy factor and $\Delta\nu_L$ the full linewidth at half height in cm^{-1}. It can be seen from the first bracketed term on the right side of Eq. (3.1) that the absorption coefficient decreases as the upper state population approaches the lower. This is the phenomenon of "bleaching" alluded to earlier. The number density dependence of the absorption coefficient is of some interest. The line width is directly proportional to number density and thus on line center ($\nu = \nu_{v,J,\Delta J}$) the absorption coefficient is independent of the total number density. On the other hand on the wings of the line ($\nu - \nu_{v,J,\Delta J} > \Delta\nu_L$) the absorption coefficient scales as the square of the number density. Thus, there can be a large variation in the pressure dependence of the absorption coefficient over the line shape.

For any given vibrational transition there are a large number of allowable rotational transitions. For example, the room temperature absorption spectrum for the $v = 0 \rightarrow 1$ transition of CO is shown in Fig. 3.1 It has been asuumed here that the pressure is such that the line width is small compared to the spacing between lines (~3.8 cm^{-1} for CO). The $v = 1 \rightarrow 2$ absorption spectrum will have a similar shape but will be shifted to somewhat longer wavelengths, as shown in Fig. 3.1, because of the molecular anharmonicity. As can be seen there is a considerable overlap between the $v = 0 \rightarrow 1$ and $v = 1 \rightarrow 2$ bands (and also with higher bands not shown) however if the line widths are small compared to the line spacing there will be none but accidental wavelength coincidences between the various lines. Thus laser light of a given wavelength can typically be absorbed by only one of the manifold of possible absorbing transitions.

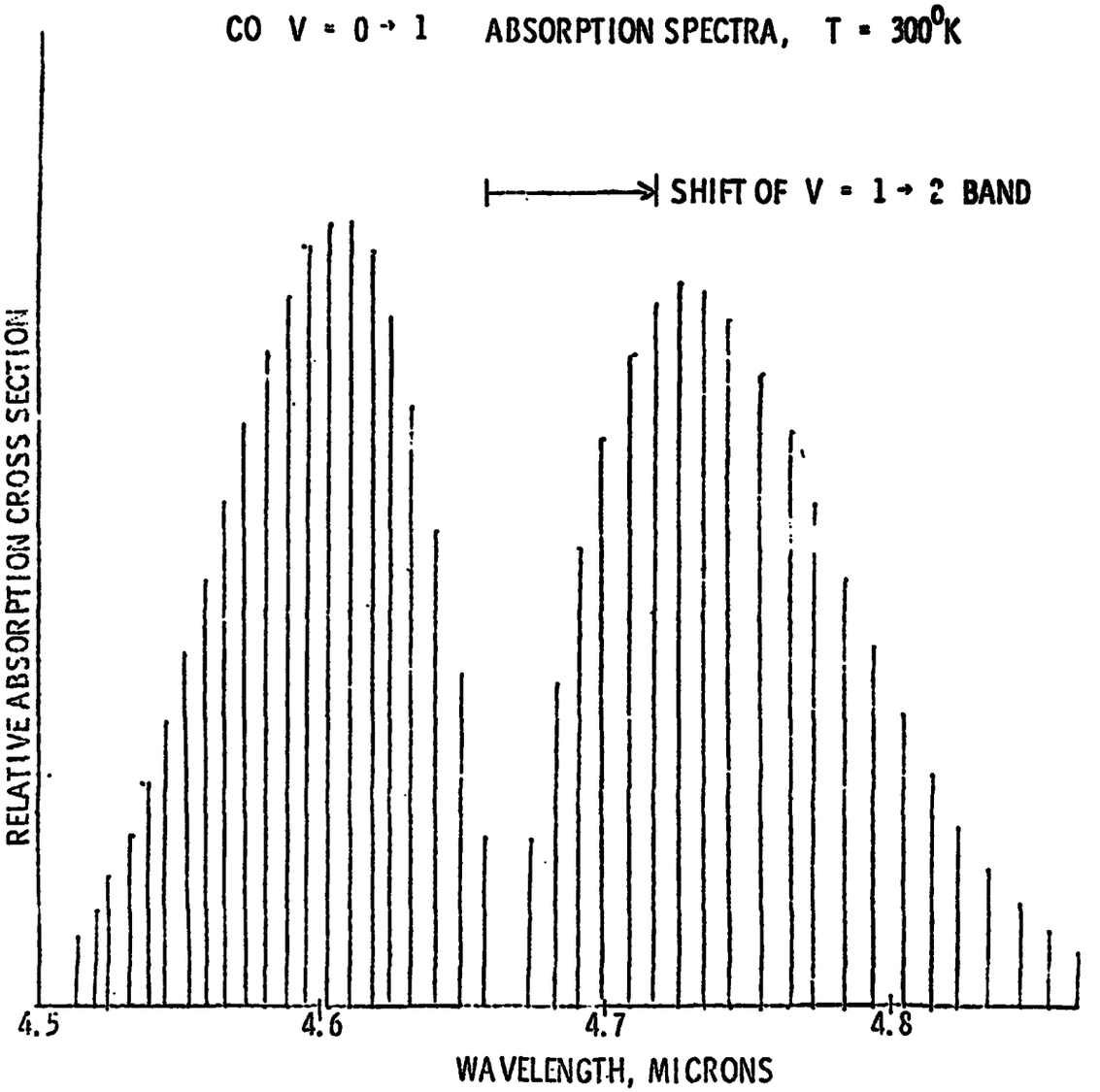

Fig. 3.1 **Room temperature, low pressure absorption spectra of the V = 0 → 1 band of CO**

This constraint will not apply at sufficiently high pressures where the line width is $\gtrsim$ to the line spacing, ($\gtrsim$ 30 atmospheres for self-broadening in CO). In this limit the molecule will absorb continuously over the wavelength region of the V/R band. The absorption coefficient at any given wavelength is no longer given directly by Eq. (3.1), but rather now involves a sum of the absorption coefficients of a number of overlapping transitions, and this sum is independent of total number density depending only upon the mole fraction of the absorbing gas.

An approximate band model has been developed for the prediction of this high pressure absorption spectra. At pressures at which the lines just overlap, occuring when $\Delta\nu_L = 2$ Be, where Be is the rotational constant of the molecule, it is assumed that the absorption spectra becomes continuous with a magnitude at any wavelength proportional to the line center value of the absorption coefficient of the transition nearest that wavelength (from Eq. (3.1)). The proportionality constant is determined by the requirement that the integration of the absorption coefficient over wavenumber be proportional to the bandstrength, i.e.,

$$S = \frac{N_o}{N} \int \alpha(\nu)\, d\nu \tag{3.2}$$

where S is the bandstrength in cm^{-2} for an absorber number density N_o, N_o is Loschmidts number and N is the number density of the absorber. The resulting absorption spectra is defined at the discrete points $\nu_{v,J,\Delta J}$ by the relationship

$$\sigma_{v-1\to v}(\nu) = \frac{\alpha_{v-1\to v}(\nu)}{N_{v-1}} = \lambda^2_{v-1,J,\Delta J} A_{v,\,v-1,\,J,\,\Delta J}$$

$$\frac{h(2J+1)}{16\pi kT} \exp\left[-\frac{J(J+1)\,hc}{kT}\left(B_e - \alpha_e\left(v+\frac{1}{2}\right)\right)\right] \tag{3.3}$$

Where N_{v-1} is the vibrational population of the absorbing state, α_e is the vibrational correction to rotation, ΔJ takes on the values ± 1 ($\Lambda = 0$) and the Einstein coefficient $A_{v,v-1,J,\Delta J}$ is related to that for the vibrational transition, $A_{v,v-1}$, by the Honle-London factors.[41] It can be seen that the absorption cross section $\sigma_{v-1,v}(\nu)$ is independent of the total number density and varies with temperature as the rotational population. Similar band models have been shown to provide a good approximation[42] to the actual high pressure absorption spectra.

This band model has been applied to the molecule CO and predictions for this case are shown in Figs. 3.2 - 3.4. In Fig. 3.2 the room temperature absorption cross section vs wavelength is shown for the lowest three vibrational transitions of CO. The cross section increases with increasing vibrational level because of the variation in the Einstein coefficient (a linear dipole moment function for CO was employed in the calculations).[43] The important feature is that, because of the large overlap between the absorption spectra for each vibrational transition, laser light of a given wavelength may be absorbed simultaneously by a number of vibrational levels. This has the effect of minimizing bleaching phenomena; for now, if a particular transition approaches the bleaching limit the upper state of that transition can also absorb the incident laser radiation.

Of more interest from the viewpoint of laser heating is the temperature variation of the absorption cross sections. This behavior will, of course, be quite sensitive to the choice of incident laser wavelength. Predictions for the absorption cross sections of the first five vibrational levels of CO over the temperature range of 200 - 3000°K are shown in Fig. 3.3. The incident laser radiation is taken to be at a wavelength of 4.755 μm, which would correspond to a P branch $v = 1 \rightarrow 0$, $J = 10$ CO laser. Although a high power CO laser of this type has not yet been developed, the results may be taken as generic for any diatomic molecule undergoing absorption at a wavelength near the center of its fundamental V/R band. As can be seen, above 300°K the absorption cross sections for the various vibrational levels are all of the same order of magnitude. The absorption cross sections for individual transitions generally tend to decrease at the higher temperatures shown because of the effect of the rotational partition function. However, absorption on the higher vibrational transitions ($v = 4 \rightarrow 5$ as well as higher transitions not shown) peak in the higher temperature region because absorption occurs in the far rotational quantum number wings of these bands. The net effect of this is that the overall molecular absorption coefficient can be relatively insensitive to temperature variations depending, of course, upon the vibrational distribution function.

A similar result is shown in Fig. 3.4 for an incident laser wavelength of 4.855 μm. This wavelength corresponds to an attainable P branch CO laser transition, $v = 3 \rightarrow 2$, $J = 8$. Since this wavelength occurs in the wing of the CO $v = 0 \rightarrow 1$ band, see Fig. 3.2, the absorption cross section for this transition initially increases rapidly with temperature. This is an important point since the upper vibrational states of CO are not significantly populated at room temperature. However, it is clear that as soon as ground state molecules are excited to the first vibrational state through absorption, excitation to higher states (including transitions to states higher than those shown in Fig. 3.4) will be quite rapid.

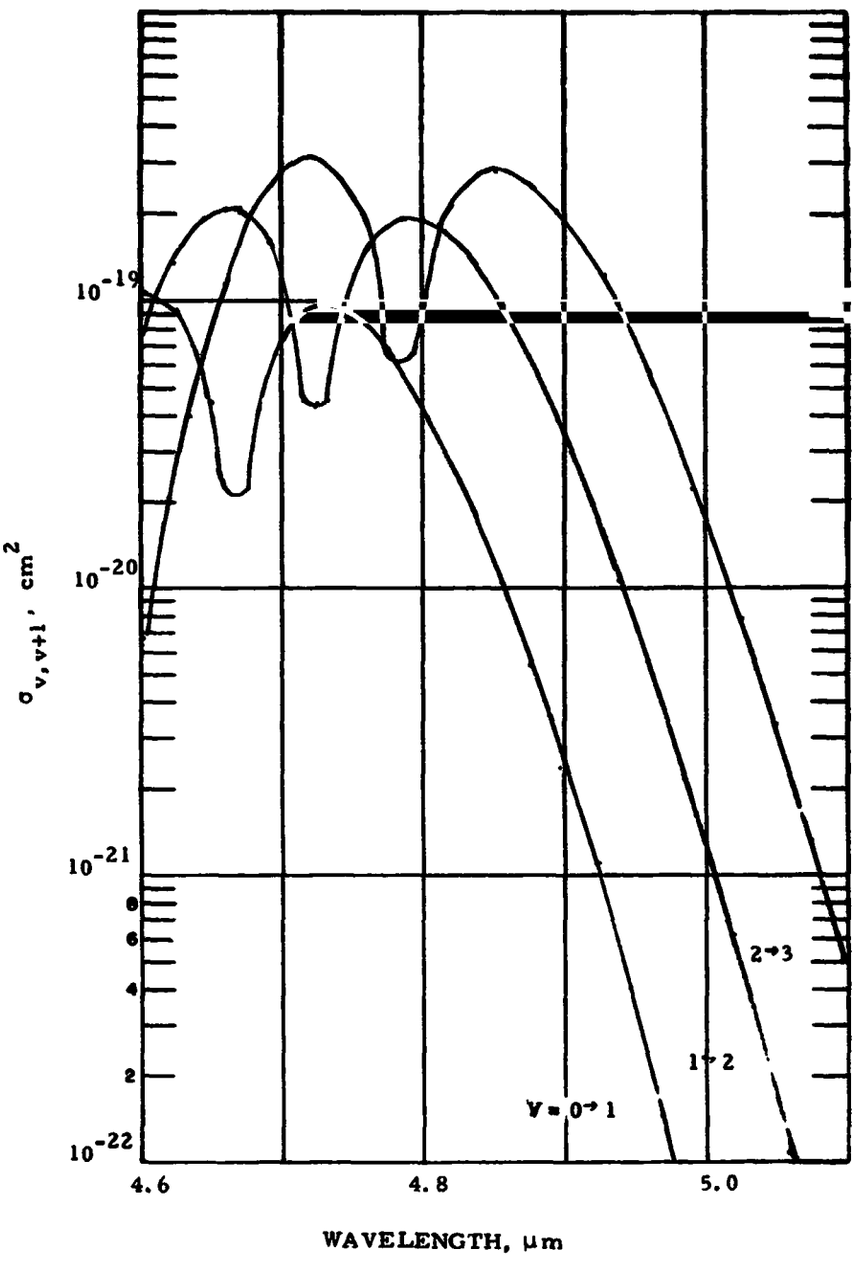

Fig. 3.2 Room temperature, high pressure absorption spectra of the V = 0 → -, V = 1 → 2 and V = 2 → 3 bands of CO.

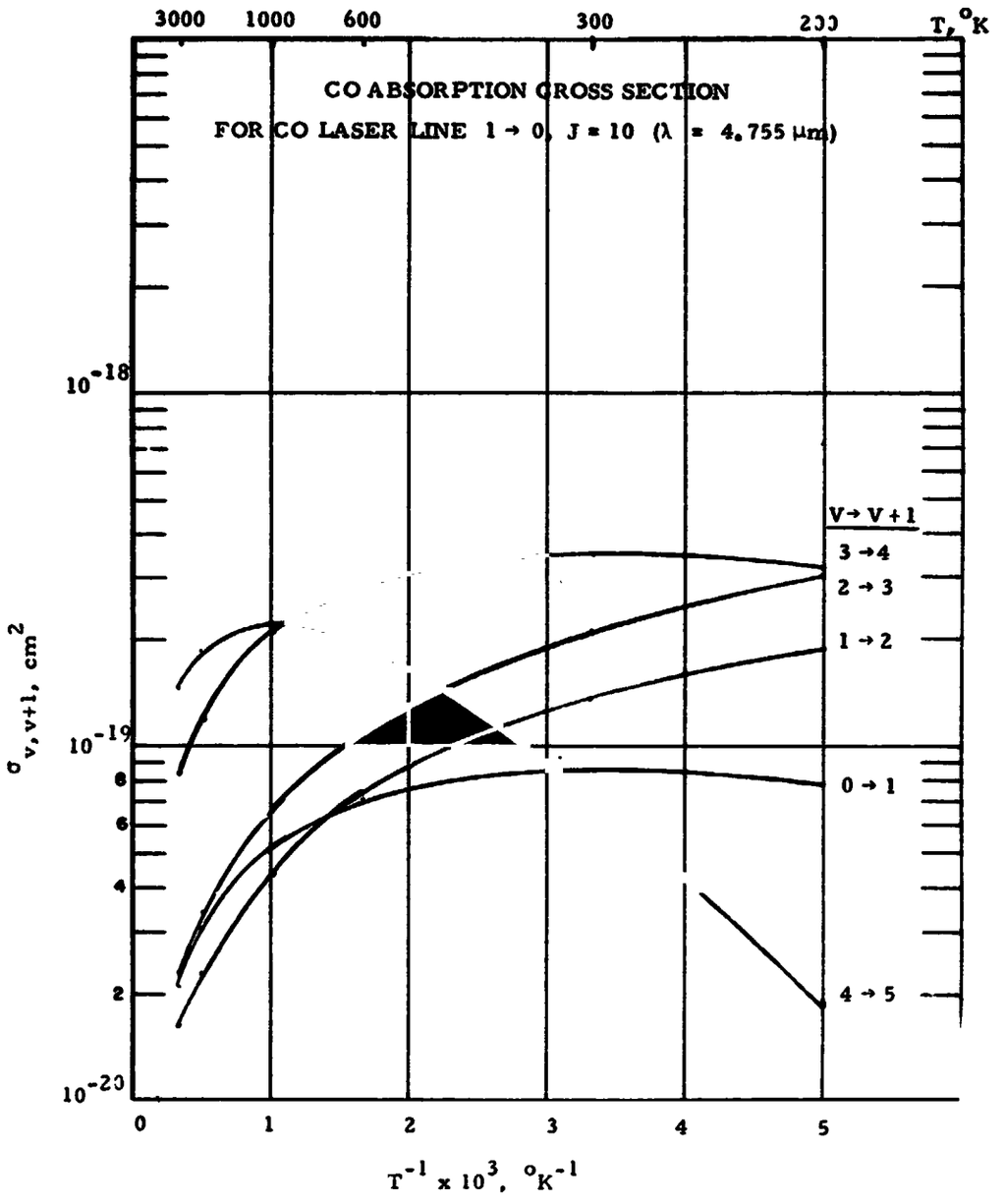

Fig. 3.3 Absorption cross section vs temperatures for the five lowest vibrational transitions in CO at a wavelength of 4.755 μm.

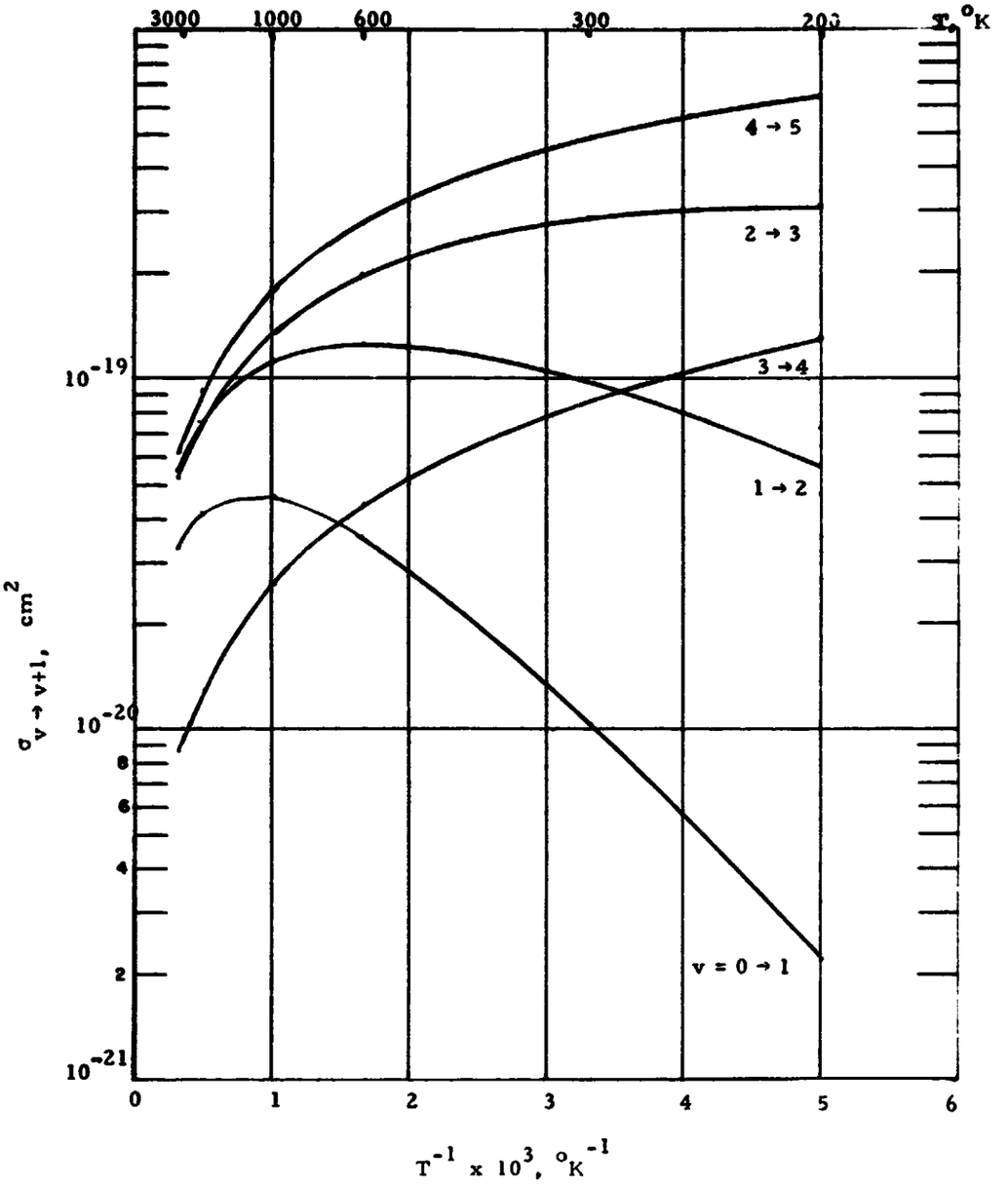

Fig. 3.4 **Absorption cross section vs temperatures for the five lowest vibrational transitions in CO at a wavelength of 4.855 μm.**

It would appear then that optimum absorption by diatomic molecules can be realized in the high pressure regime characterized by overlapping lines, since in this limit laser light of a given wavelength may be absorbed simultaneously on a number of different vibrational transitions, thus minimizing bleaching. This multiline absorption should also have the effect of flattening out the temperature variation of the total molecular absorption coefficient. It now remains to discuss techniques for the rapid conversion of the absorbed vibrational energy into translation.

3.2.1 Conversion of Vibrational Energy to Translation

The molecule CO was chosen as an example not only because its molecular properties are well defined, but also because it has a very high dissociation energy, 11.1 eV, and thus may be heated to relatively high temperatures (~ 6000°K) without introducing significant chemical effects. One disadvantage of this molecule however is that the rate constants for vibrational deactivation are quite small at temperatures below 1500°K (see for example Ref. 44). These small rate constants tend to preclude efficient coupling between the vibrational and translational modes. There are however, several atomic species such as Fe, H and O which have been shown to be efficient ($k = 10^{-13} - 10^{-12}$ cc/sec) vibrational deactivators of CO;[45-47] however, it is difficult to introduce such species into a cold gas flow.

One technique which has been considered which, although not a cyclic system, may be of some interest for systems concerned with development of thrust, etc., involves the use of a rare gas seeded with iron pentacarbonyl, $Fe(CO)_5$. $Fe(CO_5)$ absorbs in the same wavelength region as CO, its vibrational modes will strongly couple with translation and, when dissociated, produces both the absorbing molecule CO and the efficient deactivator Fe. Unfortunately, detailed modeling of this system is complicated by the fact that the low temperature absorption spectra of $Fe(CO)_5$ is not well defined.

To properly model gas laser heating by diatomic molecular absorption one requires a computer code which includes the phenomena of multiline absorption, vibration to translational (V-T) deactivation and vibration-vibration (V-V) exchange between all vibrational levels. The resulting vibrational distributions will not only be out of equilibrium with translation but can also be non-Maxwellian.

Preliminary calculations have been performed for CO neglecting V-V exchange processes and assuming that the absorption occurs on only one-rotational transition in each vibrational band. In this instance, the

master equation for the time variation in vibrational population density of a constant density gas may be written

$$
\begin{aligned}
dN_v/dt = {} & \frac{I}{h\nu}\,\sigma_{v-1\to v}(\nu)\left\{N_{v-1} - a_{v,J,\Delta J}\,N_v\right\} \\
& - \frac{I}{h\nu}\,\sigma_{v\to v+1}(\nu)\left\{N_v - a_{v+1,\,J',\,\Delta J'}\,N_{v+1}\right\} \\
& - \sum_i k_{i,v\to v-1,v}\,M_i\left\{N_v - \exp\left(\frac{-\Delta E_{v,v-1}}{kT}\right)N_{v-1}\right\} \\
& + \sum_i k_{i,\,v+1\to v}\,M_i\left\{N_{v+1} - \exp\left(\frac{-\Delta E_{v+1,\,v}}{kT}\right)N_v\right\}
\end{aligned}
\tag{3.4}
$$

where I is the laser intensity, ν is laser frequency, $\Delta E_{v,\,v-1}$ is the difference in vibrational energy between levels v, v-1 and $k_{i,\,v\to v-1}$ is the rate constant for species M_i de-activating level v to v-1. The quantities $a_{v,J,\Delta J}$ are defined as

$$
a_{v,J,-1} = \exp\left(\frac{2J\,hc\,B_e}{kT}\right), \quad \text{P branch} \tag{3.5}
$$

and

$$
a_{v,J,+1} = \exp\left(-\frac{2(j+1)\,hc\,B_e}{kT}\right), \quad \text{R branch} \tag{3.6}
$$

where J is the rotational number of the transition closest to the laser wavelength.

A calculation was performed for conditions corresponding to an initial pressure of 30 atm with 0.2% CO and 0.04% Fe in a helium bath. The laser was assumed to have an intensity of 10^6 watts/cm^2 at a wavelength of 4.855 μm, corresponding to the absorption cross sections of Fig. 3.4. The time histories of both gas absorption length and temperature for this case are shown in Fig. 3.5. As can be seen, the gas temperature

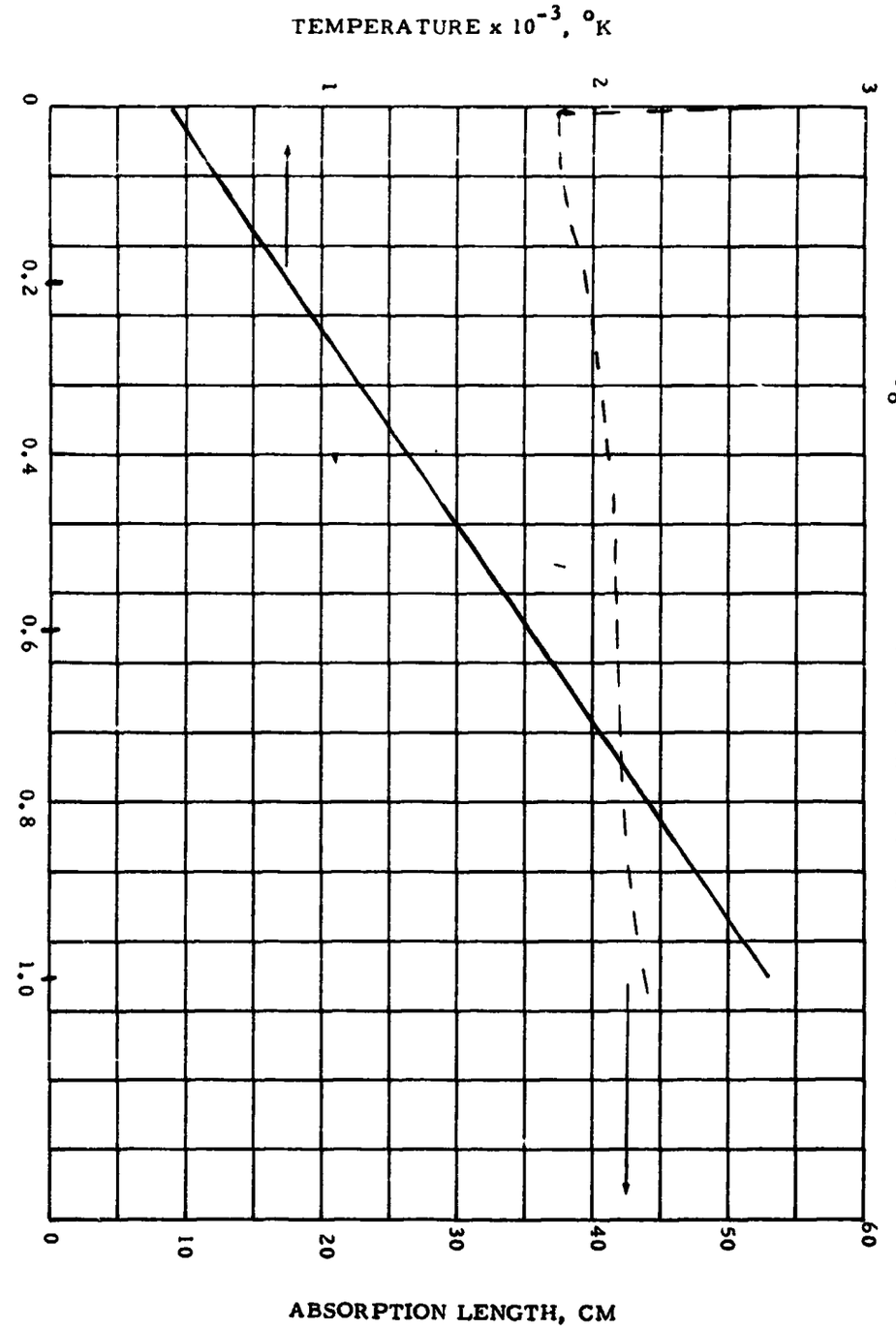

Fig. 3.5 Gas temperature and absorption length vs time. Conditions as shown.

increases essentially linearly from 400 to 3000°K and, more important, the absorption length remains approximately constant over this temperature range. The initial drop in the absorption length is caused by the early time increase in the populations of the upper vibrational states. The inclusion of V-V exchange in the modeling is not expected to produce a major change in these predictions.

3.2.2 Other Molecules

There are, of course, a number of candidate diatomic molecules which can be de-activated relatively efficiently by stable species. For example, the room temperature rate constant for self-vibrational deactivation of NO, i.e., M_i = NO, is $\sim 10^{-13}$ cc/sec (Ref. 48, among others) and furthermore the absorption spectra for NO is quite similar to that for CO. The predicted absorption spectra for the lowest two vibrational transitions of NO are shown in Fig. 3.6. The middle peaks in these spectra arise because the NO ground state is a π state and thus the Q branch is allowed. (For simplicity in this calculation a linear dipole moment was assumed and the small wavelength shift between spin states was neglected). Shown at the top of the figure are the wavelength positions of several readily attainable CO laser lines. It would appear that NO would prove to be a viable absorber for CO laser radiation.

It should be emphasized that this technique may be generally applied. In general, the radiation from most high power gas lasers which operate on vibrational transitions can be absorbed by several different diatomic molecules if the total gas density is sufficiently high to produce overlapping lines. The one major exception to this statement appears to be the 10.6 μm CO_2 laser. Although a number of the diatomic metal oxides can absorb radiation of this wavelength, these species are not readily produced under the conditions of interest. Of course this same line broadening phenomenon occurs for larger molecules. These could be reviewed to determine which species could optimally absorb CO_2 laser radiation with minimal chemical effects.

3.3 ABSORPTION BY LARGER MOLECULES

There will of course be a large number of molecules, triatomic or larger, capable of absorbing laser light of any specified wavelength. Only two examples of these will be discussed below. The first of these will be the relatively large molecule SF_6, which has been employed in many systems as an absorber of CO_2 laser radiation. The second will be the molecule CO_2, which is taken as an example of a relatively stable triatomic.

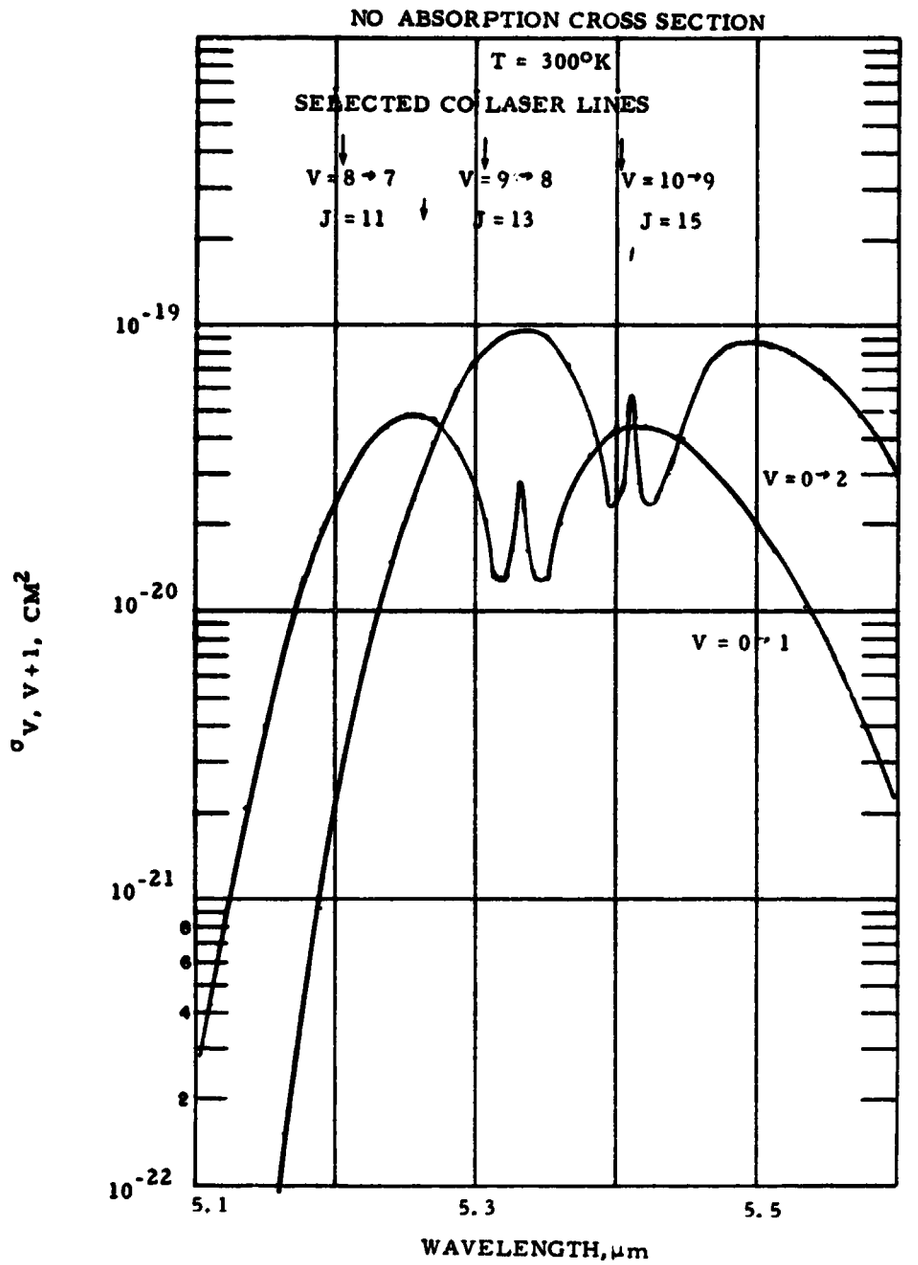

Fig. 3.6 Room temperature high pressure absorption spectra of the V = 0 → 1, V = 1 → 2 bands of NO.

The species SF_6 is an example of a large molecule whose vibrational kinetics and infrared absorption properties have been examined in some detail. SF_6 has six fundamental vibrational modes which, including degeneracies, correspond to fifteen vibrational states. Vibrational excitation in any mode is rapidly redistributed among the manifold of vibrational states, the room temperature constant for this process being $\sim 3 \times 10^{-11}$ cc/sec for collisions with rare gas atoms.[49] Vibration to translation deactivation then occurs predominantly from the lowest energy vibrational mode at a somewhat lower rate, the room temperature V-T rate constant for collisions with the rare gases being approximately 0.6×10^{-13} cc/sec.[49]

The absorption properties of SF_6 at 10.6 μm have received considerable study at temperatures near 300°K (for example, Ref. 50 and references therein). SF_6 is somewhat unusual in that the vibrational mode which absorbs the 10.6μm radiation consists of an estimated 1000 lines/cm^{-1} and at pressures above 0.5 torr the absorption becomes essentially continuous and independent of total pressure.[51] The room temperature absorption cross section[50] for SF_6 is $\sim 10^{-17}$ cm^2, a factor of 100 larger than the peak value for CO, Fig. 3.2, and thus considerably less SF_6 seeding would be required to provide any specific amount of absorption.

Anderson[50] has performed laser saturation measurements in SF_6 at room temperature and 1 atmosphere total pressure and found that significant bleaching begins to occur at laser intensities of $\sim 3 \times 10^4$ w/cm^2. (This would correspond to saturation laser intensities of $\sim 10^6$ w/cm^2 at pressures of ~30 atm.) Presumably the saturation intensity would increase with increasing temperature since it has been shown[52] that the rate constant for vibrational deactivation of SF_6 increases as $T^{4/3}$.

The temperature dependence of the SF_6 absorption coefficient is not well known and is difficult to evaluate because of the increased importance of "hot band" absorption, i.e., absorption by excited states, with increasing temperature. Anderson[50] has measured the absorption coefficient over the temperature range of 300 - 360° K and found that it decreased linearly by approximately 20% over that range. A linear extrapolation of his data would imply that the absorption coefficient goes to zero at 573°K, which is clearly a lower bound. However, as the temperature exceeds ~1000°K chemical decomposition will become important causing a gradual deterioration of the absorption process.

Thus at room temperature SF_6 absorption at 10.6 μm would appear to be as effective as the CO/Fe system at 4.855 μm which was discussed earlier and has the additional advantage that the number of absorbing molecules which must be introduced into the flow is considerably lower.

Unfortunately, gas heating to temperatures much larger than 1700°K is precluded because of thermal dissociation of the SF_6.

The vibrational kinetic behavior for SF_6 discussed above is common for many larger molecules. Energy absorbed in any given vibrational mode is first distributed among all the available vibrational modes and then converted to translation, primarily through vibrational deactivation of the lowest energy vibrational mode. For example, this behavior is observed in CO_2 although the rate constants[53] for these respective processes are lower than in SF_6.

The two fundamental vibrational bands of CO_2 are centered about 4.3 and 15 μm. The 15μ band is a relatively weak absorber. However, the band at 4.3 μm can absorb more strongly than CO. The same type of high pressure absorption analysis that was applied earlier can be used to predict the temperature dependence of the CO_2 absorption coefficient; however, the required band model would be considerably more complicated. Absorption by these bands would deteriorate at temperatures $\geq$ 2500°K because of CO_2 dissociation. However, this temperature is sufficiently high to cause thermal ionization of a seed species such as Cs.

CO_2 can also absorb at 10.6 μm in a "hot band" transition, the inverse of the CO_2 laser transition, however, the absorption coefficient for this process can vary significantly at low temperatures. Recently,[54] this absorption coefficient was measured over the temperature range of 300 - 1600°K, for the P(18) and P(20) laser lines, at pressures where the line widths were considerably less than the line spacing. The absorption coefficient increased from a value of 2×10^{-3} cm^{-1} at 300°K to a peak value of 3×10^{-2} cm^{-1} at 800°K and then decreased monotonically to 10^{-2} cm^{-1} at 1600°K. (All of these absorption coefficients are for an absorbing molecule number density of N_o.) The temperature variation between 300 - 800°K is determined primarily by the vibrational population of the lower state of the absorbing transition and thus would be similar even if the pressure were such that the lines overlapped.

There are obviously a manifold of such molecules which can be considered. However, the general phenomenology of interest from the viewpoint of laser gas heating should be adequately represented by the two examples discussed above.

3.4 SUMMARY

The conversion of laser energy to gas translational energy via absorption by the vibration/rotation bands of molecules has been examined. The most effective mechanism would appear to be absorption by the V/R

bands of diatomic molecules at sufficiently high pressures so that the lines of neighboring transitions overlap. Both the effects of gas bleaching and the temperature variation of the absorption coefficient may be minimized in this high pressure region. Unfortunately, there does not appear to be any readily produceable diatomic molecule which can absorb CO_2 laser radiation. There are a number of larger molecules which can absorb 10.6 μm radiation; however, efficient high temperature absorption by these species is precluded because of thermal dissociation. Such species may be sufficient, however, to raise the gas temperatures high enough for inverse Bremsstrahlung to be effective (~2500°K for a Cs seed).

In the kinetic analysis presented above, the bath species were assumed to be inert gases such as helium. If H_2 were the bath gas, additional kinetic mechanisms, both vibrational and chemical, would have to be considered.

4. PARTICULATE ABSORPTION

4.1 INTRODUCTION

Gas laser heating may also be achieved through seeding the gas flow with particulates. In this case, the particles absorb the laser radiation, are heated to temperatures above that of the bath and then thermally conduct heat to the surrounding gas. The advantages of this technique are threefold; (1) the absorption can be spectrally continuous, allowing use of any laser wavelength, (2) the absorption process is efficient in a cold gas and only a small percentage of the absorbed energy remains in the particle, and (3) the conversion of the absorbed energy to gas translational energy is relatively rapid. The basic disadvantages are (1) the more complicated system required for reliable particle formation and injection, and (2) particle vaporization at increased temperatures.

In the sections below, the phenomenology of particle heating will be described. The discussion includes a review of the absorption properties of particulates and preliminary modeling of the gas heating rate.

4.2 DISCUSSION

4.2.1 Particulate Absorption

Large particles, defined as particles of characteristic size much larger than the wavelength of the incident radiation, will absorb as gray bodies, with an absorption cross section defined as

$$\sigma_A(\lambda) = \epsilon_\lambda 4\pi R^2 \qquad (4.1)$$

where ϵ_λ is the wavelength dependent material emissivity and R is particle radius. For simplicity, the particles are assumed to be spherical. As the particle size approaches the wavelength of the incident radiation, the particle causes a perturbation to the electromagnetic field about it, and the full Mie theory[55] is required to predict the absorption cross section. In this instance σ_A is a complicated function of particle radius and the complex index of refraction, $M = n - in'$ of the material. A simplification in Mie theory results when the particle size is considerably smaller than the wavelength of incident radiation (Rayleigh absorption). Under these conditions the absorption cross section is given by

$$\sigma_A(\lambda) = - \frac{8\pi^2 R^3}{\lambda} I_m \left\{ \frac{M^2 - 1}{M^2 + 2} \right\} . \qquad (4.2)$$

This type of absorption is referred to as volume absorption and generally written as

$$\sigma_A = \alpha V , \qquad (4.3)$$

where V is the particle volume and α is the volume absorption coefficient defined by

$$\alpha = \frac{6\pi}{\lambda} I_m \left\{ \frac{M^2 - 1}{M^2 + 2} \right\} \qquad (4.4)$$

The maximum absorption efficiency per unit mass loading of particulates is achieved in the limit of volume absorption since in this limit the total volume, rather than surface area, of the particle is involved in the absorption process. It is clear that volume absorption will apply if the particle is optically "thin". This condition is satisfied when

$$\alpha R < 1 \qquad (4.5)$$

The value of α can vary considerably depending on material, wavelength and temperature. Generally speaking, the volume absorption coefficient for elemental materials such as C, Al, etc. will have a relatively smooth spectral variation whereas the absorption by more complex materials such as SiO_2, Al_2O_3, etc. can be highly structured spectrally. An example of the infrared spectral variation of α at room temperature for two such materials is shown in Fig. 4.1. The data for soot is taken from the work of Volz[56] while that for SiO_2 is taken from Steyer et al.[57] In the visible the values of α for carbon are approximately a factor of 6 higher[58] while on the other hand SiO_2 is essentially transparent.

The characteristic absorption length for particles in the volume absorption limit is given by

$$L = (4/3\ \pi R^3\ N_p\ \alpha)^{-1} \qquad (4.6a)$$

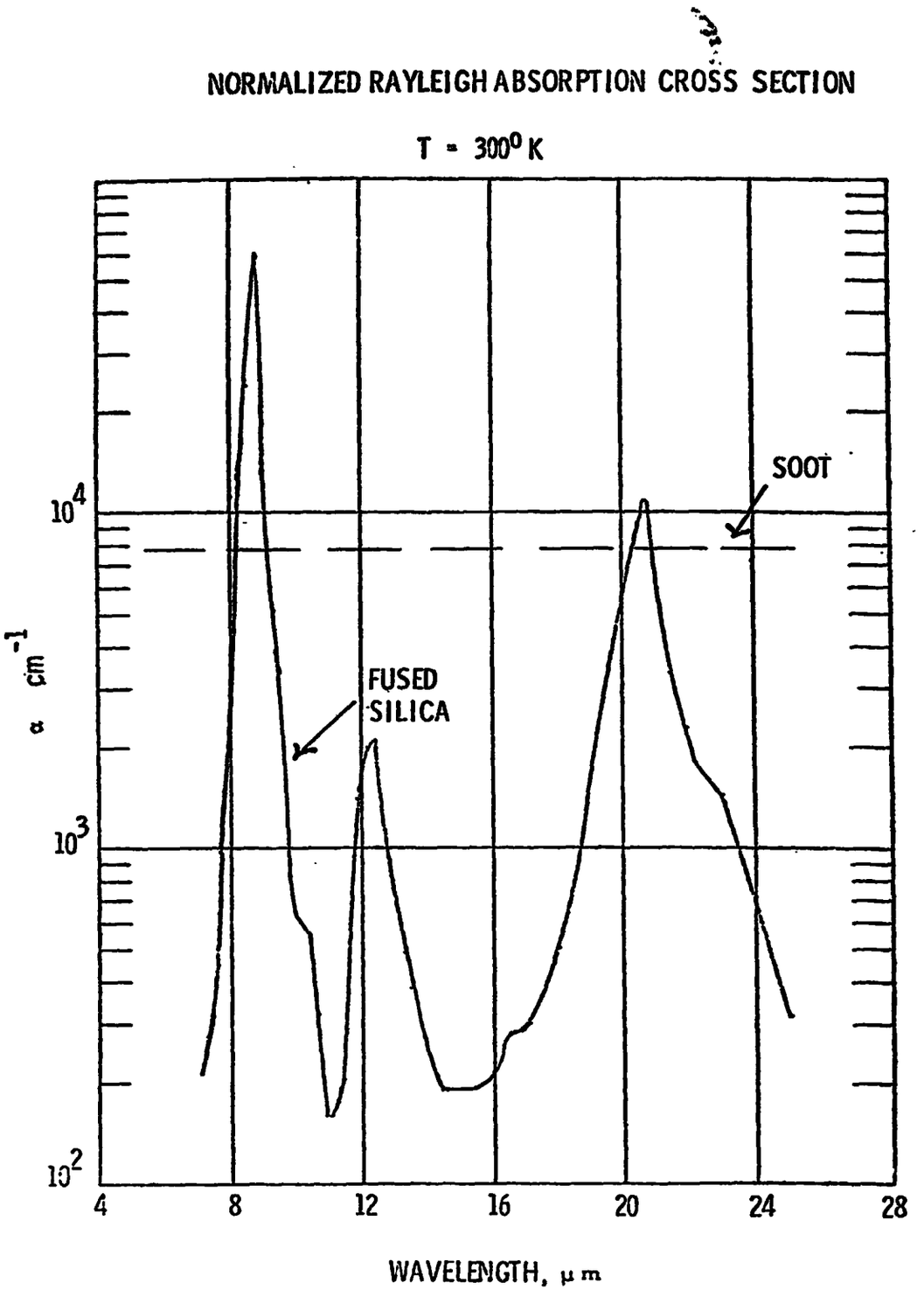

Fig. 4.1 Volume absorption coefficient vs. wavelength for soot and fused silica. T = 300°K.

or

$$L = \rho_p/(M_p \alpha) \tag{4.6b}$$

where N_p, M_p and ρ_p are particle number density, mass loading and specific density respectively. Thus, to achieve an absorption length of 10 cm for nominal values of $\alpha = 2 \times 10^3$ cm^{-1}, $\rho_p = 2$ gms/cc would require a particle mass loading, M_p, of 10^{-4} gms/cc. Furthermore, from condition (4.5), the particle radius would have to be less than 5 μm. This mass loading would correspond to ~1% of the typical reservoir densities under consideration and to a particle density of $N_p \sim 10^{-5}/R^3$ (for example, 10^7 particles/cc for a radius of 1 μm).

4.3 HEATING PHENOMENOLOGY

Upon absorption of laser radiation, the particle will heat up, thermally conduct heat to the surrounding gas, melt and vaporize (the small effect of thermal radiation is neglected). The effect of vaporization is only important at higher temperatures, approaching the boiling point of the material, and will be neglected in the following analysis.

For the case of a constant density gas, the differential equations defining the temperature history of a laser irradiated particle and the gas surrounding it may be written

$$4/3\,\pi R^3 I\alpha = 4/3\,\pi R^3 \rho_p\, d\,(C_{p_p}\, T_p)\, dt - 4\pi R^2\, k\, \partial T_p/\partial r \Big|_R \qquad r = R \tag{4.7}$$

$$\rho\, \partial \left[C_v (T - \overline{T})\right] / \partial t - \vec{\nabla} \cdot (k \vec{\nabla} T) = 0 \qquad r > R \tag{4.8}$$

where vaporization and melting have been neglected and the temperature field within the droplet has been taken to be spatially uniform. In these equations, I is the laser intensity, C_{p_p} is the particle specific heat, k is the gas thermal conductivity, C_v is the gas specific heat at constant volume and $\overline{T}$ is the average gas temperature. If the gas is seeded with N_p particles/cc of radius R, the rate of increase of average gas temperature is given by

$$\rho d\,(C_v\, \overline{T})/dt = -4\pi R^2\, N_p\, k\, \partial T/\partial r \Big|_R \tag{4.9}$$

Unfortunately, the quantities α, C_{p_p}, C_v and k are themselves functions of temperature and it is not possible to derive analytic solutions for Eqs. (4.7)-(4.9). Nonetheless, one can examine the qualitative behavior of these equations by examining their solution when the former quantities are constant.

Under this assumption, one can readily show that the solution to Eq. (4.8) for $r \approx R$ is given by[59]

$$T - \overline{T} \approx \frac{R}{r} (T_p - \overline{T}) , \tag{4.10}$$

whence

$$\partial T_p / \partial r \Big|_R = - (T_p - \overline{T})/R \tag{4.11}$$

If relationship (4.11) is substituted into Eq. (4.7), it can be shown that the solutions of Eq. (4.7), (4.9) are

$$T_p - \overline{T} = (T_p - \overline{T})_{s.s.} \left[1 - \exp (-t/\tau) \right] \tag{4.12}$$

and

$$d\overline{T}/dt = \frac{L^{-1} I}{\rho C_v (1 + F C_{p_p}/C_v)} \left[1 - \exp (-t/\tau) \right] \tag{4.13}$$

where F is the relative mass loading, M_p/ρ, and

$$(T_p - \overline{T})_{s.s.} = \frac{R^2 I \alpha}{3k (1 + F C_{p_p}/C_v)} \tag{4.14}$$

$$\tau = \frac{\rho_p C_{p_p} R^2}{3k (1 + F C_{p_p}/C_v)} \tag{4.15}$$

In essence the difference between the particle and average gas temperature approaches a steady state value, Eq. (4.14), in a characteristic irradiation time τ. Furthermore, the gas heating rate approaches a constant value with the same time constant τ. After this time, the absorbed laser energy is converted almost totally into gas heating.

There are a number of constants which must be specified in evaluating Eqs. (4.12)-(4.15). Room temperature values for several representative absorbing materials and bath gases are given in Table 4.1. (C_{pp}, C_v and k all increase with increasing temperature. The largest variation is in C_{pp} which in the case of carbon increases by a factor of ~3 between 300 and 2000°K). It can be seen from these representative values that the quantity $F\, C_{pp}/C_v$, which is found in Eqs. (4.13)-(4.15), will be significantly smaller than unity for the relative mass loadings of interest, $\sim 10^{-2}$, and can be neglected.

The efficiency of gas heating by particulate absorption may be optimized by minimizing both $(T_p - \bar{T})_{s.s.}$ and τ. It can be seen from Eqs. (4.14)-(4.15) that this may be accomplished by reducing the particle size. For a specific numerical example, if $I = 10^6$ w/cm^2, $a = 2 \times 10^3$ cm^{-1}, and k, ρ_p, C_{pp} took on characteristic values then a particle of size 0.3 μm would approach steady state in a characteristic time of ~5 μsec with a temperature differential, $T_p - \bar{T}$, of ~500°K. These latter two quantities would decrease by an order of magnitude if the particle size were reduced to 0.1 μm.

It is particularly important to minimize the temperature differential since the above relationships break down as the particle temperature approaches the boiling point. In this limit the major portion of the absorbed energy is lost in the latent heat of vaporization rather than in gas heating (a similar, but transient, effect occurs at the melting point). More importantly, as the particle vaporizes and thus reduces in size, the absorption coefficient decreases. Finally, if the bath gas is not inert, undesirable heterogeneous chemical reactions may occur at the particle surface. The boiling temperatures for several absorbing materials are listed in Table 4.1. Vaporization effects, however, may be important at temperatures considerably below these values.

Interestingly enough, although the particle absorption coefficient will decrease as vaporization occurs, the vapor species may provide alternate absorption mechanisms. For example, at temperatures $\gtrsim 2500$°K, the dominant metal oxide vapors will be diatomic. Absorption in the V/R bands of these molecules occurs at ~10 μm, i.e., in the wavelength region of the CO_2 laser. Furthermore, the vapor species, or their elemental components, can have ionization potentials significantly lower than that of the bath gas (see Table 4.1), thus allowing equilibrium inverse Bremsstrahlung absorption to dominate at lower temperatures than in the pure bath gas.

TABLE 4.1

TYPICAL PARTICULATE PROPERTIES

(T = 300° K)

Species	ρ, $\frac{gm}{cc}$	C_p $\frac{cal}{gm^oK}$	~ Boiling Point, ^oK	Dominant Vapor Species	Metal Ionization Potential, eV
Al_2O_3	3.7	0.17	3800	AlO	6.0
C (Graphite)	2.3	0.17	4500	C	11.3
Fe_2O_3	5.2	0.15		FeO	7.9
SiO_2 (Fused)	2.3	0.22	3600	SiO	8.1
W	19.3	0.034	6200	W	8.0

Gases	C_v $\frac{cal}{gm-^oK}$	k, $\frac{cal}{cm-sec-^oK}$
H_2	2.5	3.9×10^{-4}
He	0.75	3.4×10^{-4}

To summarize, although detailed predictions require a full computer solution, it has been demonstrated that particulate absorption can provide a viable method for high efficiency laser gas heating. The technique is optimized by utilizing very small particles, $\lesssim 0.3\ \mu m$ with typical mass loadings of order 10^{-4} gms/cc. Although the effects of vaporization are deleterious to particulate absorption, the vapor species themselves can provide alternate absorption mechanisms and it is conceivable that a system design which would allow "complete" vaporization of the particles could be very efficient. The basic disadvantage of particulate seeding is the equipment requirements for particle production.

5. ANALYSIS OF FLOW AND STABILITY REQUIREMENTS

5.1 INTRODUCTION

This section presents the part of our program that was directed toward fluid dynamic considerations for laser heated flows. Specifically, the objective was to develop the capability to predict the thermodynamic and fluid dynamic properties resulting from the radiation heating of a nozzle flow. In addition, the capability to determine the stability of the resulting flow field is considered essential to a study of the efficiency of converting laser energy to a high velocity flow.

For simplicity, a quasi one-dimensional nozzle flow is considered (Fig. 5.1). In this nozzle geometry the laser radiation will enter either through a window at the flow inlet plane or through the exhaust at the exit plane. The flow is considered to be that of a perfect gas, and the absorbed laser energy will be considered to be instantaneously converted to temperature (i.e. equilibrium flow). The equations of motion will be solved to obtain steady state solutions, and a "local" stability analysis will be performed to determine how stable the absorption zone is to small disturbances.

The stability of radiatively heated flows along with suggestions for acoustic wave amplification by radiative absorption have been examined to some extent by many authors.[60] In general, the technique for determining stability is to obtain a steady state solution and then super-impose an infinitesimal disturbance. The disturbance is composed of a number of discrete partial fluctuations, each of which consists of a wave. For each single oscillation of the disturbance the sign of roots to the resulting characteristic equations are examined as a function of intensity and wave number to determine when stable solutions can be expected. Since the steady flow properties are not constant in a one-dimensional nozzle flow, when waves are introduced, the corresponding boundary value problem is rather difficult. However, much can be learned about wave propagation without solving the full boundary value problem, and information can be extracted from a study of the modified dispersion relation. To obtain the modified dispersion relation in inhomogeneous media the actual disturbance is approximated by harmonic functions over a small distance (small compared with the characteristic lengths associated with the gradients of the flow) and, hence, the analysis is only an accurate

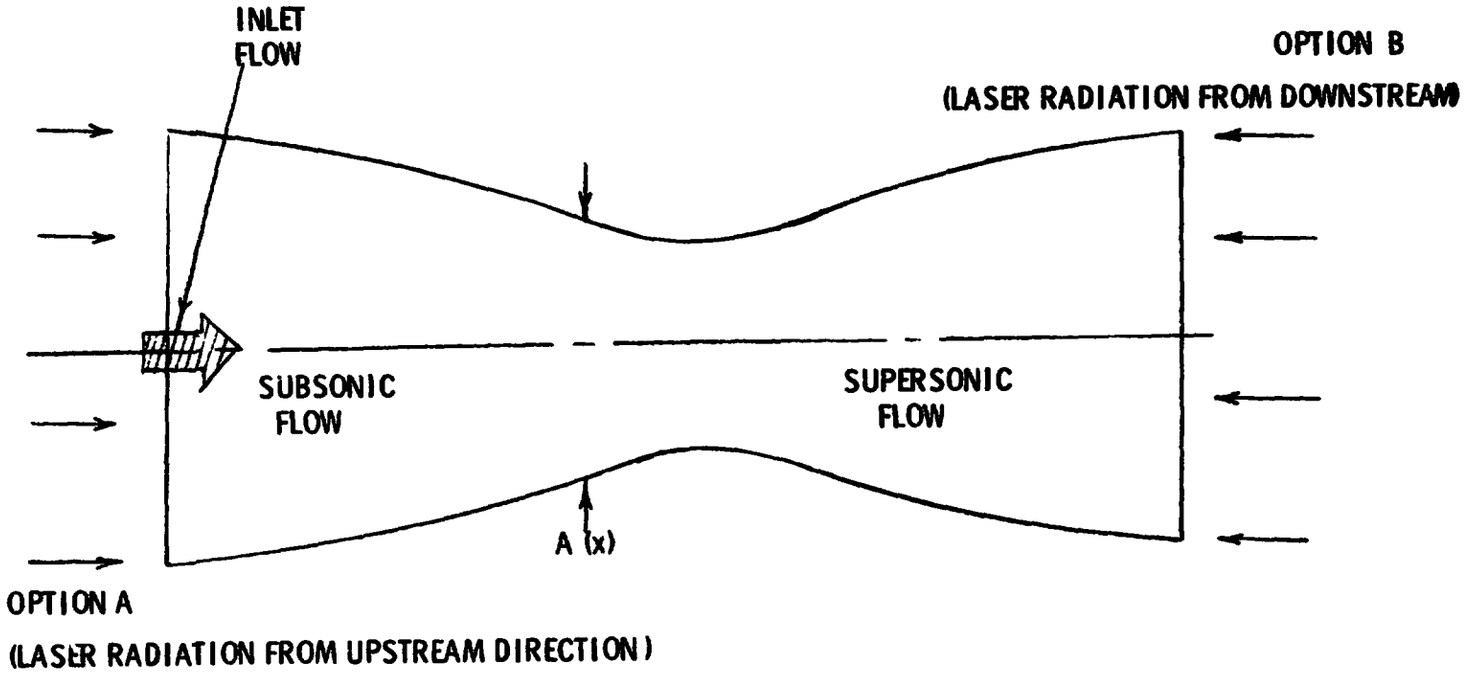

Fig. 5.1 Nozzle configuration for laser heated flow

description "locally". This procedure is commonly used in problems of this type (e.g. Monsler[61] has examined the stability of radiative heating between two infinite plates).

5.2 STEADY NOZZLE FLOWS WITH LASER-ENERGY ADDITION

Consider a one-dimensional flow through a nozzle of variable area ratio that is heated by laser radiation (Fig. 5.1). The laser beam enters either through the nozzle inlet plane in the same direction as the flow (termed Option A) or through the exhaust plane in the direction opposite to the flow direction (termed Option B). The governing equations for quasi-one-dimensional steady flow without viscous dissipation, diffusion and thermal conduction, but including absorption of laser radiation are:

$$\begin{cases} \dfrac{d}{dx}\left(\rho u A\right) = 0 \\ \dfrac{dp}{dx} + \rho u \dfrac{du}{dx} = 0 \\ \rho u \left(\dfrac{dh}{dx} + u \dfrac{du}{dx}\right) = \dfrac{1}{A} \dfrac{d(IA)}{dx} \\ \dfrac{d}{dx}\left(IA\right) = \mp IA k_\nu \end{cases} \tag{5.1}$$

where ρ is the density, u is the velocity, A is the area, p is the pressure, h is the enthalpy, I the local laser intensity and k_ν is the absorption coefficient. The minus and plus signs correspond to Option A and B, respectively.

Calculations will be carried out for generalized absorption coefficients of the form

$$k_\nu = K_o \rho^n T^m$$

where K_o is a constant, T is the gas temperature, and n and m are constants characterizing the absorber. It is useful to write the governing equations in terms of an optical depth τ defined as[62]

$$\tau = \int_0^x k_\nu \, dx \tag{5.2}$$

Inserting Eq. (5.2) into the radiative transfer equation (last of Eq. (5.1), we can immediately integrate the resulting equation to obtain the laser power distribution (IA) as a function of optical depth τ. The result for Option A is

$$IA = I_i A_i e^{-\tau}$$

where the subscript i denotes conditions at the nozzle inlet plane, and for Option B

$$IA = I_e A_e e^{\tau - \tau_e}$$

where the subscript e denotes conditions at the exhaust exit plane. When τ is introduced into the remaining equations, and the dependent variables are made dimensionless with ρ_i, u_i, h_{s_i}...etc., where i denotes inlet conditions, Eqs. (5.1) become

$$\frac{d}{d\tau}\left(\rho u A\right) = 0 \tag{5.3}$$

$$\frac{dp}{d\tau} + \rho u \frac{du}{d\tau} = 0 \tag{5.4}$$

$$\frac{d}{d\tau}\left(h + \frac{u^2}{2}\right) = \Gamma e^{-\tau} \quad \text{(Option A)}$$

$$\frac{d}{d\tau}\left(h + \frac{u^2}{2}\right) = \Gamma e^{\tau - \tau_e} \quad \text{(Option B)} \tag{5.5}$$

The important parameter Γ, which is the ratio of laser power to the initial total energy flux of the flow, is defined as

$$\Gamma = \frac{I\!P}{\rho_i u_i A_i h_{si}}$$

where $I\!P$ is the incident laser power (equal to $I_i A_i$ for Option A and $I_e A_e$ for Option B) and h_{si} is the initial stagnation enthalpy. Since Eq. (5.5) is directly integrable, the increase in stagnation enthalpy, $h_s = h + u^2/2$, becomes

$$\begin{aligned} h_s &= 1 + \Gamma\left(1 - e^{-\tau}\right) \qquad \text{(Option A)} \\ h_s &= 1 + \Gamma\, e^{-\tau_e}\left(e^{\tau} - 1\right) \qquad \text{(Option B)} \end{aligned} \tag{5.6}$$

It can be seen from Eqs. (5.2) and (5.6) that without proper absorption coefficient tailoring, the absorption will take place close to the inlet or exit plane. The actual physical location will depend upon the chosen nozzle configuration and can only be determined by inverting Eq. (5.2).

The equation of state

$$p = \rho R T$$

together with Eqs. (5.3) - (5.4) provide the equations for the remaining variables ρ, u, and T. A general method for solutions to this system of equations may be employed.[63] The governing equations can be combined to yield a relationship which governs the Mach number variation through the nozzle

$$\frac{dM^2}{d\tau} = \frac{F(M^2, \tau)}{1 - M^2} \tag{5.7}$$

and

$$F\left(M^2, \tau\right) = \left[1 + \frac{(\gamma-1)}{2} M^2\right] M^2 \left[(1 + \gamma M^2) \frac{1}{h_s} \frac{dh_s}{d\tau} - \frac{2}{A} \frac{dA}{d\tau}\right]$$

where M is the Mach number. For convenience, the nozzle contour is

chosen to be the one parameter nozzle configuration used by Buonadonna et al,[64]

$$\frac{A}{A_i} = 1 + \left(\frac{A_T}{A_i} - 1\right) \frac{(1+d-\tau)\, e^{\tau} - (1+d)}{e^{d} - (1+d)} \qquad (5.8)$$

where A_i is the initial area ($\tau = 0$) and A_T is the throat area located at $\tau = d$. The calculations are not restricted to this configuration and can easily be extended to any arbitrary nozzle shapes. As a matter of fact, the nozzle contour will be one of the parameters to be examined when optimizing the power conversion efficiency.

Eq. (5.7)together with Eq. (5.6) and (5.8) are used to obtain the Mach number distribution along the nozzle axis. Since we are only interested in a flow which accelerates from subsonic (convergent section) to supersonic (divergent section), the solution is obtained by first locating the position corresponding to the singular point when $F(M^2, \tau) \to 0$ as $M \to 1$, and then integrating upstream and downstream to get the desired Mach number distribution.

Example calculations for area ratio $A_T/A_i = 0.3$, $d = 2$ and $\Gamma = 0, 1, 2$ and 4 are obtained for two nozzle shapes as shown in Figs. 5.2 and 5.3. It can be seen that when heating is in the supersonic flow region (Option B) the flow is driven toward $M = 1$. This is because the nozzle area ratio does not increase rapidly enough in the supersonic region to compensate the laser heating effect. It can be shown that a faster increase in area ratio in the divergent section provides a continuous increase in Mach number distribution. The above results are presented in terms of the optical depth τ. However, they can easily be transformed to the actual physical space for given absorbers by inverting Eq. (5.2).

Knowing the Mach number profile for a nozzle configuration with known inlet conditions and laser power, the complete steady state solution for ρ, u, and T, can be calculated. Further examples of such calculations are discussed in Section 5.4.

5.3 STABILITY ANALYSIS

Due to the inhomogeneous nature of the one-dimensional nozzle flow, it is difficult to solve the resulting eigenvalue problem when perturbations are superimposed upon the steady solution. Hence, the "local" stability analysis described in Section 5.1 will be applied to determine the stability at each point along the nozzle.

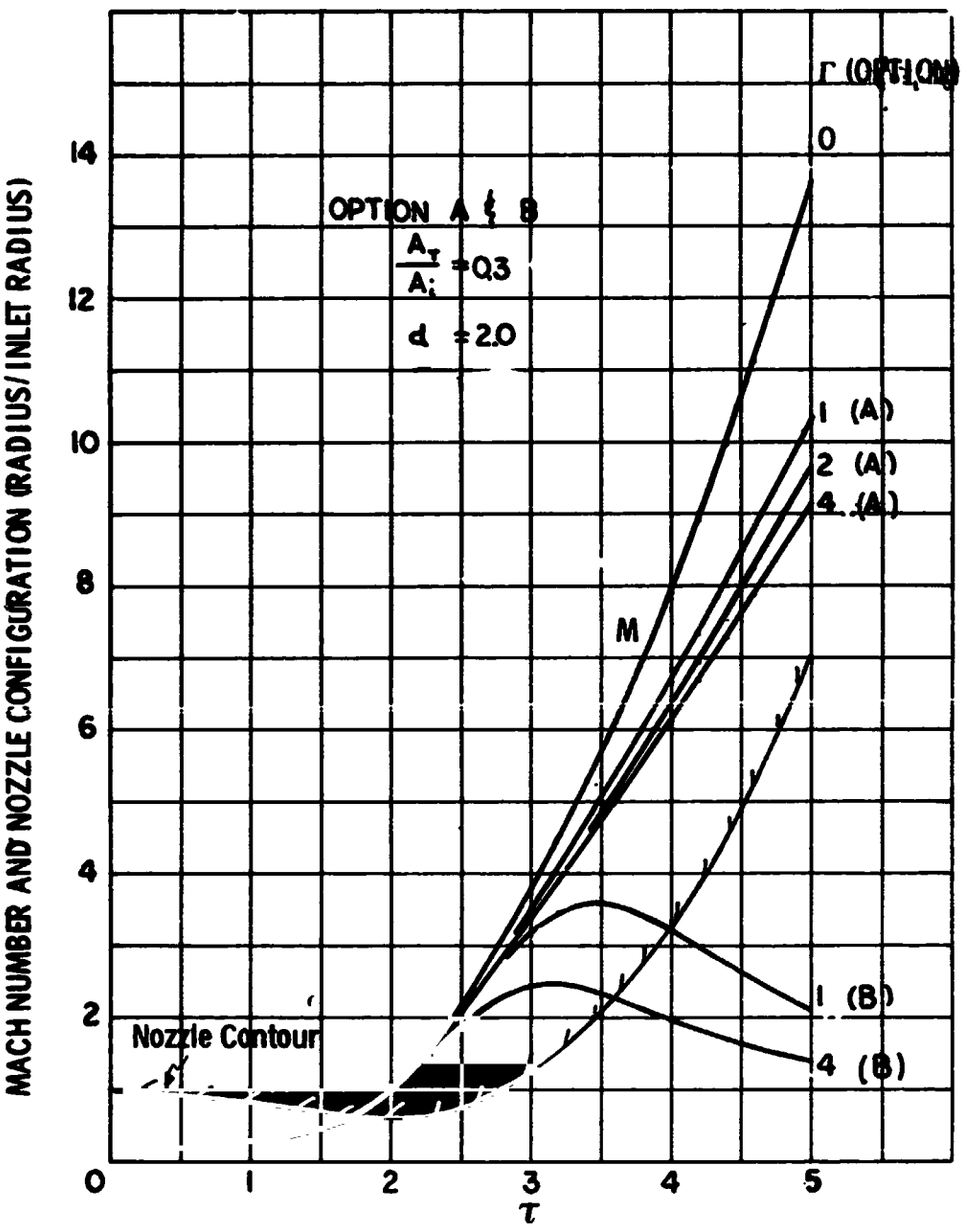

Fig. 5.2 Mach number distribution along a nozzle with convex contour

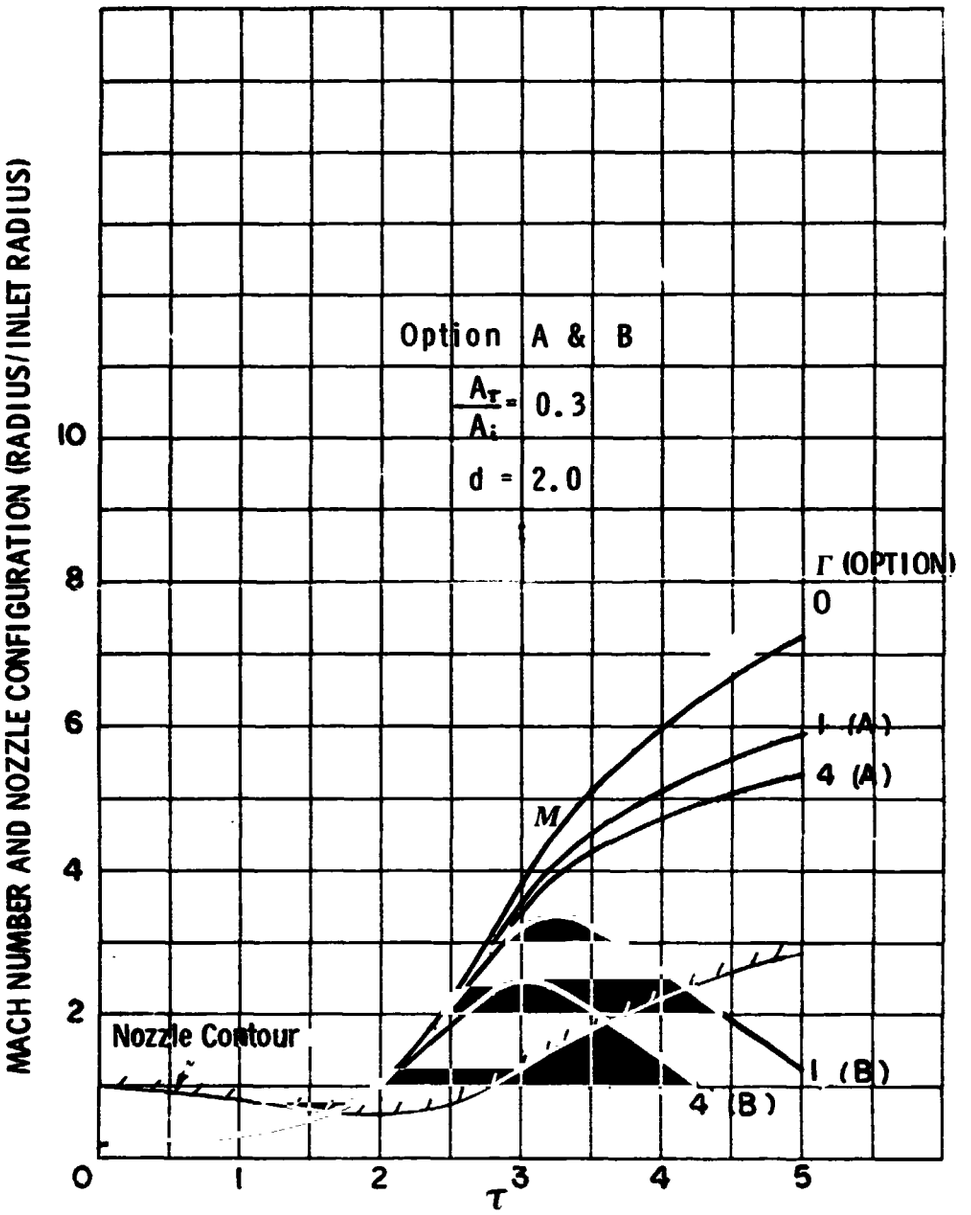

Fig. 5.3 Mach number distribution along a nozzle with concave contour

Since the superimposed wave disturbance will be time dependent, it is necessary to write the full unsteady one-dimensional equations with heat addition. They are

$$\frac{\partial \rho}{\partial t} + \frac{\partial (\rho u)}{\partial x} + \frac{\rho u}{A}\frac{dA}{dx} = 0 \tag{5.9}$$

$$\rho \frac{\partial u}{\partial t} + \rho u \frac{\partial u}{\partial x} + \frac{\partial p}{\partial x} = 0 \tag{5.10}$$

$$\rho \frac{\partial}{\partial t}\left(h + \frac{u^2}{2}\right) + \rho u \frac{\partial}{\partial x}\left(h + \frac{u^2}{2}\right) - \frac{\partial p}{\partial t} = \frac{l_i A_i}{A} k_\nu e^{-\tau} \tag{5.11}$$

$$\frac{dp}{p} = \frac{d\rho}{\rho} + \frac{dT}{T} \tag{5.12}$$

$$\frac{\partial \tau}{\partial x} = k_\nu = K_o \rho'' T^m \tag{5.13}$$

Only Option A has been considered; however, the analysis can be easily extended to Option B. For simplicity, the pressure is eliminated from Eq. (5.10) and (5.11) by means of Eq. (5.12). Now we have 4 equations for 4 unknowns (ρ, u, T and τ), and can proceed to superimpose disturbances upon the previously obtained steady flow field by assuming

$$\begin{aligned} \rho &= \rho_o (x) + \rho' (x,t) \\ u &= u_o (x) + u' (x,t) \\ T &= T_o (x) + T' (x,t) \\ \tau &= \tau_o (x) + \tau' (x,t) \end{aligned} \tag{5.14}$$

where ρ_o, T_o, u_o, and τ_o are the known steady state variables and the primes indicate small perturbations, i.e., $\rho' \ll \rho_o$. Neglecting the second or higher order terms and substituting Eq. (5.14) into Eqs. (5.9) - (5.13), yield a linear set of equations for the perturbation quantities.

$$
\left\{
\begin{aligned}
&\frac{\partial \rho'}{\partial t} + u_o \frac{\partial \rho'}{\partial x} + \rho_o \frac{\partial u'}{\partial x} + \left(\frac{\partial u_o}{\partial x} + \frac{u_o}{A} \frac{dA}{dx} \right) \rho' + \left(\frac{\partial \rho_o}{\partial x} + \frac{\rho_o}{A} \frac{dA}{dx} \right) u' = 0 \\
&\rho_o \frac{\partial u'}{\partial t} + R T_o \frac{\partial \rho'}{\partial x} + \rho_o u_o \frac{\partial u'}{\partial x} + R \rho_o \frac{\partial T'}{\partial x} + \left(u_o \frac{\partial u_o}{\partial x} + R \frac{\partial T_o}{\partial x} \right) \rho' + \rho_o \frac{\partial u_o}{\partial x} u' \\
&\qquad + R \frac{\partial \rho_o}{\partial x} T' = 0 \\
&- R T_o \frac{\partial \rho'}{\partial t} + \rho_o u_o \frac{\partial u'}{\partial t} + \rho_o u_o^2 \frac{\partial u'}{\partial x} + c_p \rho_o u_o \frac{\partial T}{\partial x} \\
&+ \left(c_p u_o \frac{\partial T_o}{\partial x} + u_o^2 \frac{\partial u_o}{\partial x} \right) \rho' + \left(c_p \rho_o \frac{\partial T_o}{\partial x} + 2 \rho_o u_o \frac{\partial u_o}{\partial x} \right) u' = \\
&\qquad \frac{I_i A_i'}{A} k_{\nu_o} e^{-\tau_o} \left(\frac{n}{\rho_o} \rho' + \frac{m}{T_o} T' - \tau' \right) \\
&\frac{\partial \tau'}{\partial x} - \frac{k_{\nu_o} n}{\rho_o} \rho' - \frac{k_{\nu_o} m}{T_o} T' = 0
\end{aligned}
\right. \qquad (5.15)
$$

It can be seen in Eqs. (5.15) that the coefficients are only functions of the steady state solutions and hence, for the sake of simplicity, the above equations are non-dimensionalized with respect to the steady state variables, i.e.,

$$
\bar{\rho} = \frac{\rho'}{\rho_o} ; \quad \bar{u} = \frac{u'}{u_o} ; \quad \bar{x} = \frac{x}{L} \text{ and } \bar{t} = \frac{t u_o}{L}
$$

where the characteristic length L is taken to be $1/k_{\nu_o}$. With this normalization, Eq. (5.15) becomes:

$$
\left\{
\begin{aligned}
&\frac{\partial \bar{\rho}}{\partial \bar{t}} + \frac{\partial \bar{\rho}}{\partial \bar{x}} + \frac{\partial \bar{u}}{\partial \bar{x}} + \left[\frac{\partial}{\partial \bar{x}}\left(\ell n\, u_o + \ell n\, A\right)\right]\bar{\rho} + \left[\frac{\partial}{\partial \bar{x}}\left(\ell n\, \rho_o + \ell n A\right)\right] \\
&\frac{\partial \bar{u}}{\partial \bar{t}} + \alpha\, \frac{\partial \rho}{\partial \bar{x}} + \frac{\partial \bar{u}}{\partial \bar{x}} + \alpha\, \frac{\partial \bar{T}}{\partial \bar{x}} + \left(\frac{\partial}{\partial \bar{x}}\, \ell n\, u_o + \alpha\, \frac{\partial}{\partial \bar{x}}\, \ell n\, T_o\right)\bar{\rho} \\
&\qquad + \left(\frac{\partial}{\partial \bar{x}}\, \ell n\, u_o\right)\bar{u} + \left(\alpha\, \frac{\partial}{\partial \bar{x}}\right)\bar{T} = 0 \\
&-\alpha\, \frac{\partial \rho}{\partial \bar{t}} + \frac{\partial \bar{u}}{\partial \bar{t}} + \frac{\alpha}{\gamma-1}\, \frac{\partial \bar{T}}{\partial \bar{t}} + \frac{\partial \bar{u}}{\partial \bar{x}} + \frac{\gamma}{\gamma-1}\, \alpha\, \frac{\partial \bar{T}}{\partial \bar{x}} + \left[\frac{\gamma}{\gamma-1}\, \alpha\, \frac{\partial}{\partial \bar{x}}\, \ell n\, T_o\right. \\
&\qquad \left. + \frac{\partial}{\partial \bar{x}}\, \ell n\, u_o - \Gamma' n\right]\bar{\rho}' + \left(\frac{\gamma}{\gamma-1}\alpha\, \frac{\partial}{\partial \bar{x}}\, \ell n\, T_o + 2\, \frac{\partial}{\partial \bar{x}}\, \ell n\, u_o\right)\bar{u} \\
&-\Gamma' m\, \bar{T} + \Gamma'\, \tau' = 0 \\
&\frac{\partial \tau'}{\partial \bar{x}} - n\bar{\rho} - m\, \bar{T} = 0
\end{aligned}
\right. \tag{5.16}
$$

where γ is the ratio of specific heats, $\alpha = R\, T_o / u_o^{\,2}$ and

$$\Gamma' = \Gamma\, \frac{h_{so}}{u_o^{\,2}}\, e^{-\tau_o}$$

The steady state flow field is assumed to be influenced at a given location by a disturbance which is composed of a number of discrete partial fluctuations (harmonics). The perturbations representing a single oscillation of the disturbance are assumed to be of the form

$$\bar{\rho} = \hat{\rho}\,(\Omega,\ K)\ e^{i\,(K\bar{x} - \Omega\bar{t})}$$

$$\bar{u} = \hat{u}\,(\Omega,\ K)\ e^{i\,(K\bar{x} - \Omega\bar{t})}$$

$$\bar{T} = \hat{T}\,(\Omega,\ K)\ e^{i\,(K\bar{x} - \Omega\bar{t})} \qquad (5.17)$$

$$\bar{\tau} = \hat{\tau}\,(\Omega,\ K)\ e^{i\,(K\bar{x} - \Omega\bar{t})}$$

The nondimensional wave number K is a real quantity and $\lambda = 2\pi L/K$ is the wavelength of the disturbance. The quantity, Ω, is the complex dimensionless frequency

$$\Omega = \Omega_r + \Omega_i$$

where $\Omega_r\ u_o/L$ is the frequency of the partial oscillation and $\Omega_i\ u_o/L$ (the amplification factor) determines the degree of amplification or damping. The disturbances are damped if $\Omega_i < 0$ and the steady-state flowfield is stable, whereas for $\Omega_i > 0$ disturbances will grow. The velocity of propagation of the wave in the x-direction (phase velocity) is given by

$$C = \frac{\Omega_r}{K}\ u_o$$

Substituting Eq. (5.17) into Eqs. (5.16), we obtain

$$\left\{\begin{array}{l}
\left(\dfrac{\partial}{\partial\bar{x}}\ell n\,u_o + \dfrac{\partial}{\partial\bar{x}}\ell n\,A - i\Omega + iK\right)\hat{\rho} + \left(\dfrac{\partial}{\partial\bar{x}}\ell n\,\rho_o + \dfrac{\partial}{\partial\bar{x}}\ell n\,A + iK\right) \\
\left(\dfrac{\partial}{\partial\bar{x}}\ell n\,u_o + \alpha\dfrac{\partial}{\partial\bar{x}}\ell n\,T_o + i\alpha K\right)\hat{\rho} + \left(\dfrac{\partial}{\partial\bar{x}}\ell n\,u_o - i\Omega + iK\right)\hat{u} \\
\qquad + \left(\alpha\dfrac{\partial}{\partial\bar{x}}\ell n\,\rho_o + i\alpha K\right)\hat{T} = 0 \\
\left(\dfrac{\gamma}{\gamma-1}\alpha\dfrac{\partial}{\partial\bar{x}}\ell n\,T_o + \dfrac{\partial}{\partial\bar{x}}\ell n\,u_o - \Gamma' n + i\alpha\Omega\right)\hat{\rho} + \left(\dfrac{\gamma}{\gamma-1}\alpha\dfrac{\partial}{\partial\bar{x}}\ell n\,T_o\right. \\
\left.\quad + 2\dfrac{\partial}{\partial\bar{x}}\ell n\,u_o - i\Omega + iK\right)u + \left(-\Gamma' m - i\dfrac{\alpha}{\gamma-1}\Omega + i\dfrac{\gamma}{\gamma-1}\alpha K\right)\hat{T} + \Gamma''\hat{\tau} = 0 \\
-n\hat{\rho} - m\hat{T} + iK\hat{\tau} = 0
\end{array}\right. \qquad (5.18)$$

The above equation can be written as

$$A\,\overline{V} = 0$$

where A is a 4 x 4 matrix and $\overline{V}$ is the unknown column vector, i.e.,

$$\overline{V} = (\hat{\rho}, \hat{u}, \hat{T}, \hat{\tau})^{-1}$$

In order that the solution exists, the determinant of A must vanish. Hence

$$\begin{vmatrix} \frac{\partial}{\partial \bar{x}} \ell n\ u_o + \frac{\partial}{\partial \bar{x}} \ell n\, A - i\Omega + iK & \frac{\partial}{\partial \bar{x}} \ell n\ \rho_o + \frac{\partial}{\partial \bar{x}} \ell n A + iK & 0 & 0 \\ \frac{\partial}{\partial \bar{x}} \ell n\ u_o + \alpha \frac{\partial}{\partial \bar{x}} \ell n\ T_o + i\alpha K & \frac{\partial}{\partial \bar{x}} \ell n\ u_o - i\Omega + i\,K & \alpha \frac{\partial}{\partial \bar{x}} \ell n\ \rho_o + i\alpha K & 0 \\ \frac{\gamma}{\gamma-1} \alpha \frac{\partial}{\partial \bar{x}} \ell n\ T_o + \frac{\partial}{\partial \bar{x}} \ell n\ u_o & \frac{\gamma}{\gamma-1} \alpha \frac{\partial}{\partial \bar{x}} \ell n\ T_o + 2 \frac{\partial}{\partial \bar{x}} \ell n\, u_o - \Gamma' m & \Gamma' & \\ -\Gamma' n + i\alpha\Omega & -i\ \Omega + iK & -\frac{i\alpha}{\gamma-1}\Omega + i \frac{\gamma\alpha}{\gamma-1} K & \\ -n & 0 & -m & iK \end{vmatrix} = 0 \qquad (5.19)$$

This expression is the modified dispersion relation and provides the relationship between the real K and the complex Ω. The method of solution is to assume K and, then, solve for the complex Ω (3 roots) at each location along the nozzle. This corresponds to applying an infinitesimal wave of wavelength $2\pi L/K$ at each location and examining whether the disturbance will grow, ($\Omega_i > 0$) or decay ($\Omega_i < 0$). The locus of $\Omega_i = 0$ define contours of neutral stability. The states of neutral stability can be one of two kinds. For $\Omega_r = 0$ the amplitudes of a small disturbance can grow or be damped aperiodically (stationary mode) when $\Omega_r \neq 0$ (oscillatory mode) the theory tells us not only what the mode of disturbance is that will be manifested at onset of instability, but also the characteristic frequency of the oscillations.

5.4 RESULTS AND DISCUSSION

Sample solutions to Eq. (5.19) have been obtained for Option A (laser beam from upstream) and for one nozzle configuration (d = 2 and $A/A_i = 0.5$). These calculations can also be carried out for Option B as well as for other nozzle shapes.

For this particular nozzle configuration calculations have been done for $\Gamma = 0$, 1, 2 and 5. As shown in Fig. 5.4, the Mach number distributions are plotted as functions of τ_o, the steady-state flowfield optical depth. For a given absorber (and hence a known absorption coefficient) one can readily transform these results into the physical space by inverting Eq. (5.2). In Figs. 5.5 - 5.7 the density, the velocity and the temperature distributions versus τ_o are presented. As can be expected, the acceleration of the flow near the inlet region, where the absorption takes place, increases with increasing laser power. As the laser power is increased, the temperature also increases and the density decreases such that the pressure profile becomes a weak function of Γ. For these steady-state flowfields disturbances were superimposed and solutions to Eq. (5.19) were examined to determine whether such disturbances grow or decay in the nozzle.

Stability maps for $\Gamma = 1$, 2 and 5 are presented in Figs. 5.8 - 5.10. These results are for the generalized absorption coefficient of the form

$$k_\nu \sim \rho^n T^m \tag{5.20}$$

and a sample case where the absorber is fully ionized such that n = 2 and m = -3/2 is computed. Therefore, absorption is via inverse Bremsstrahlung. For this case the gas must first be heated to a temperature high enough to produce a sufficient number of electrons for this absorption process to dominate (unless a discharge is initiated via gas breakdown).

Since the governing equations have been normalized with respect to the steady-state solution, the above results are only functions of Γ (ratio of laser power to the initial steady energy flux), the nozzle shape and the generalized form of absorption coefficient.

In Figs. 5.8 - 5.10 a nondimensional wavenumber is plotted against the optical depth in the steady state flowfield, and contours of $\Omega_i = 0$ are drawn. These contours form the boundary between stable and unstable regions in wavenumber space. At each nozzle location (corresponding to a specific τ_o) the shaded zone indicates the range of wave numbers which result in growing disturbances. For example, in Fig. 5.8 at $\tau_o = 1$ disturbances with wavenumbers in the range $0.1 \leq K \leq .37$ and $6 \leq K \leq 4.5 \times 10^4$ will grow; however, at $\tau_o = 1.7$ disturbances with wavenumbers over the entire range will be damped. It must be remembered that this analysis will not tell us whether a disturbance, which is initiated

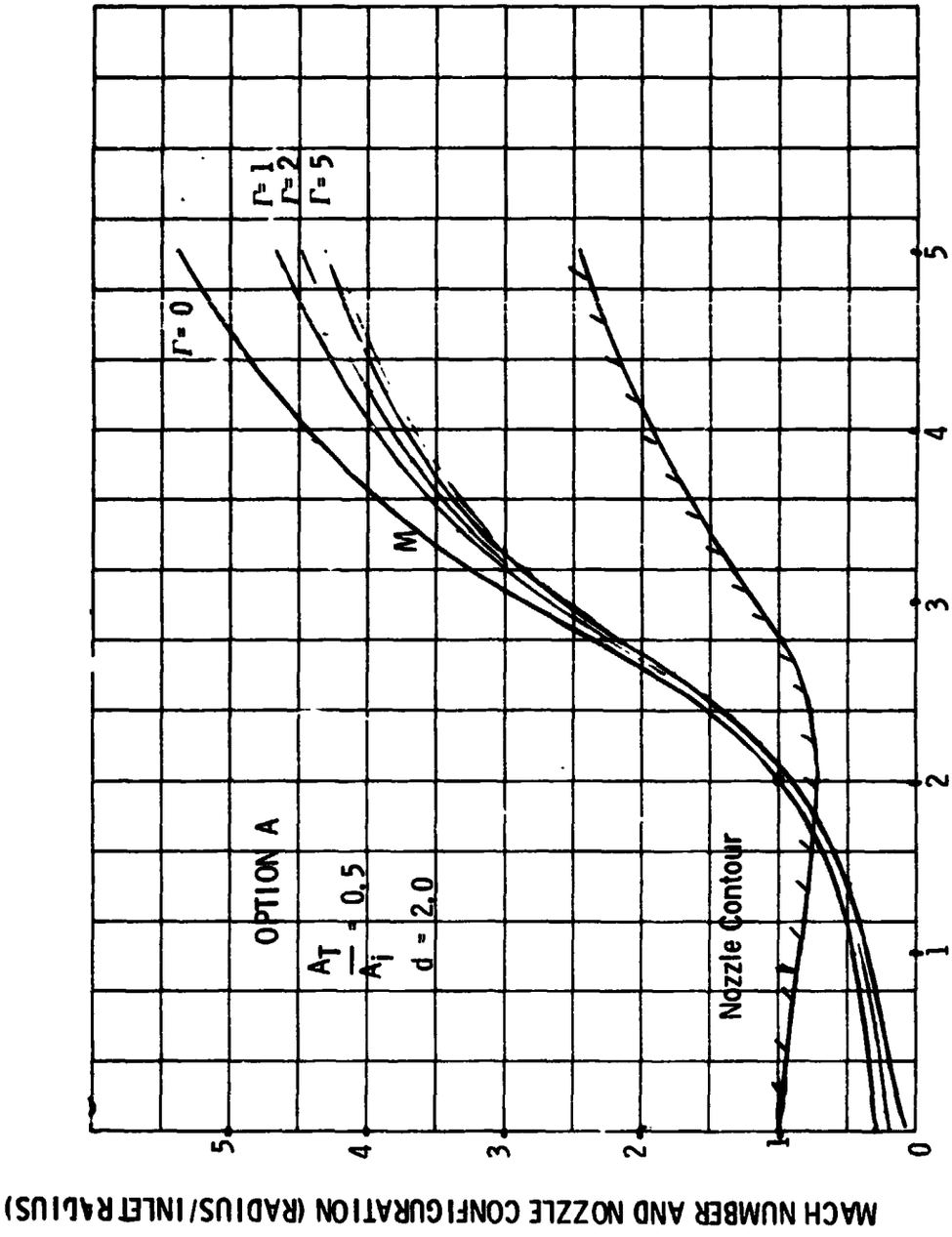

Fig. 5.4 Mach number distribution along the nozzle

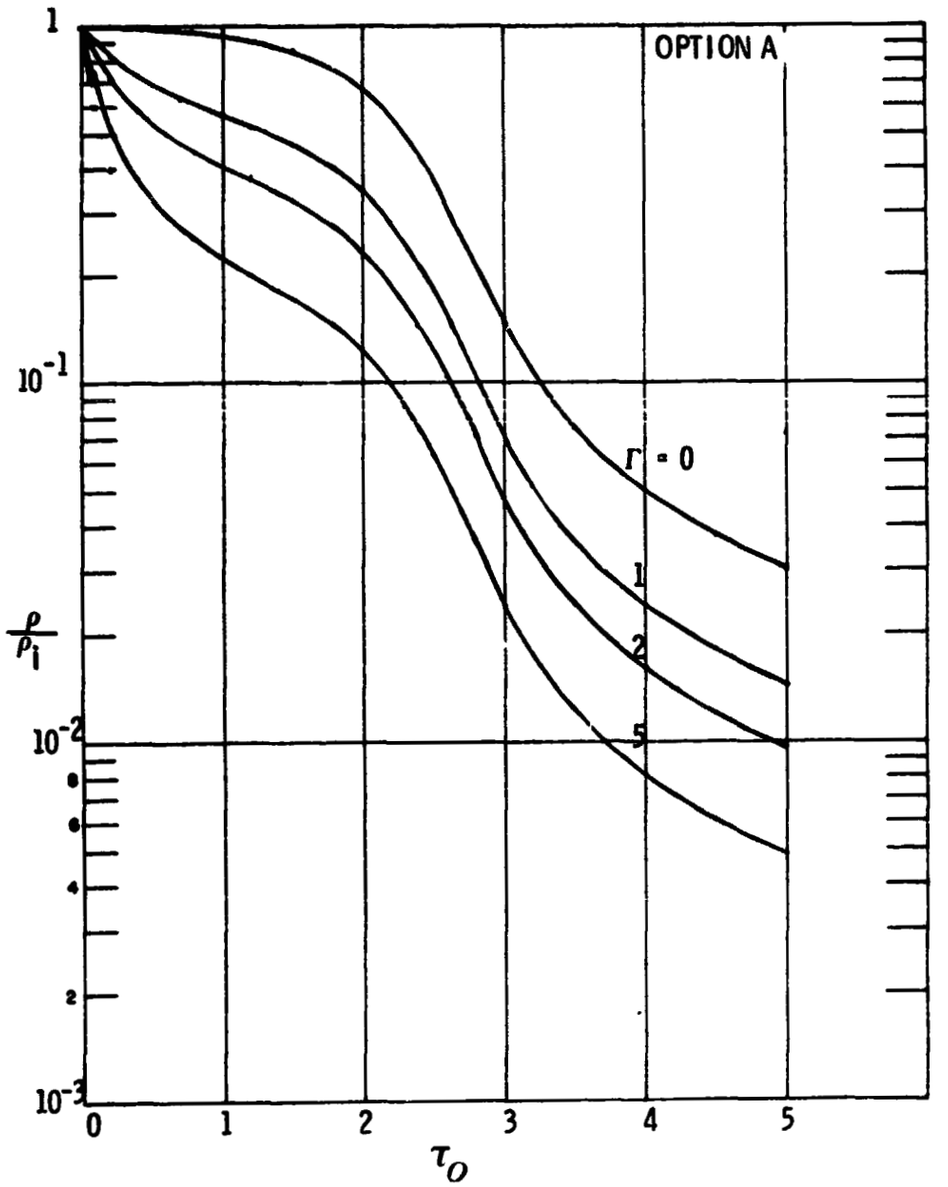

Fig. 5.5 Dimensionless density

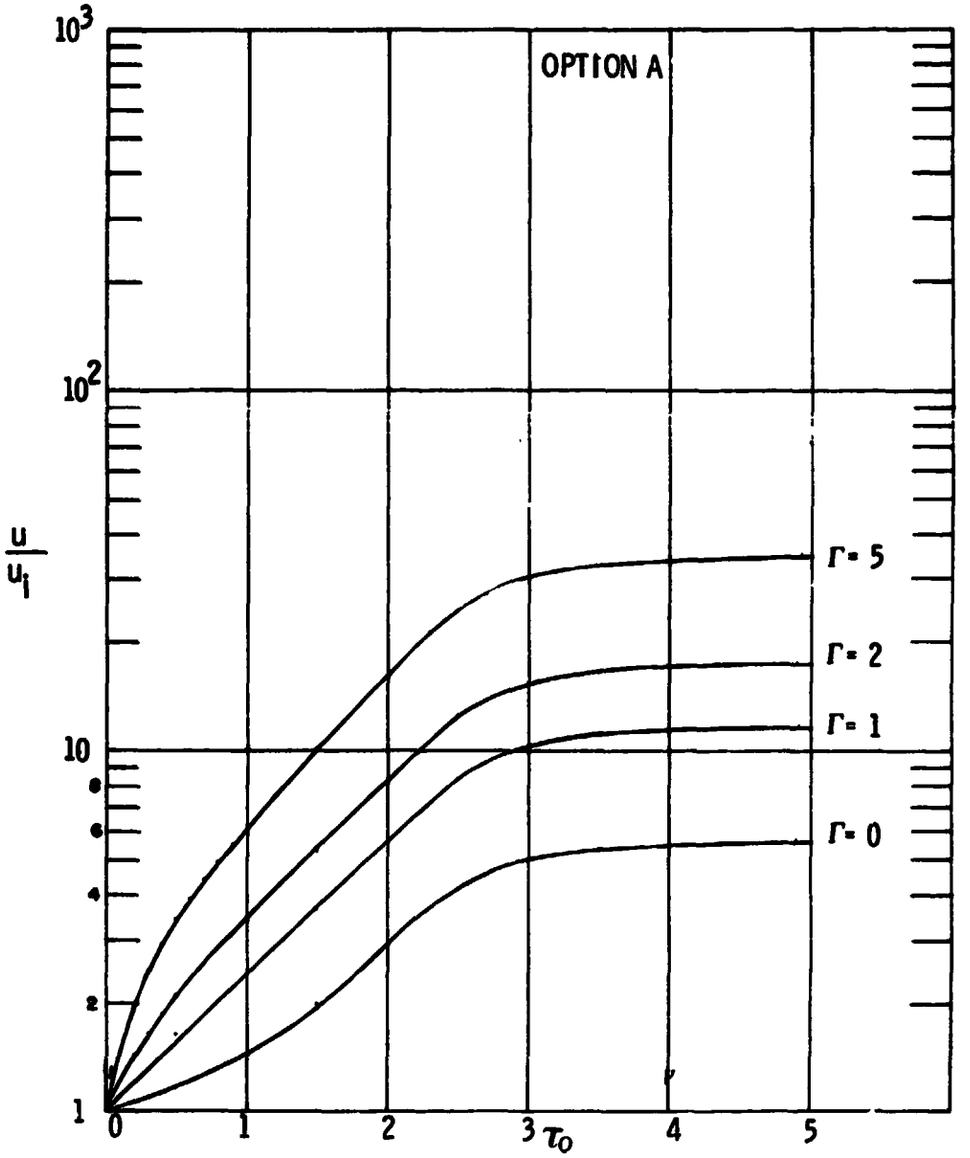

Fig. 5.6 Dimensionless velocity distribution

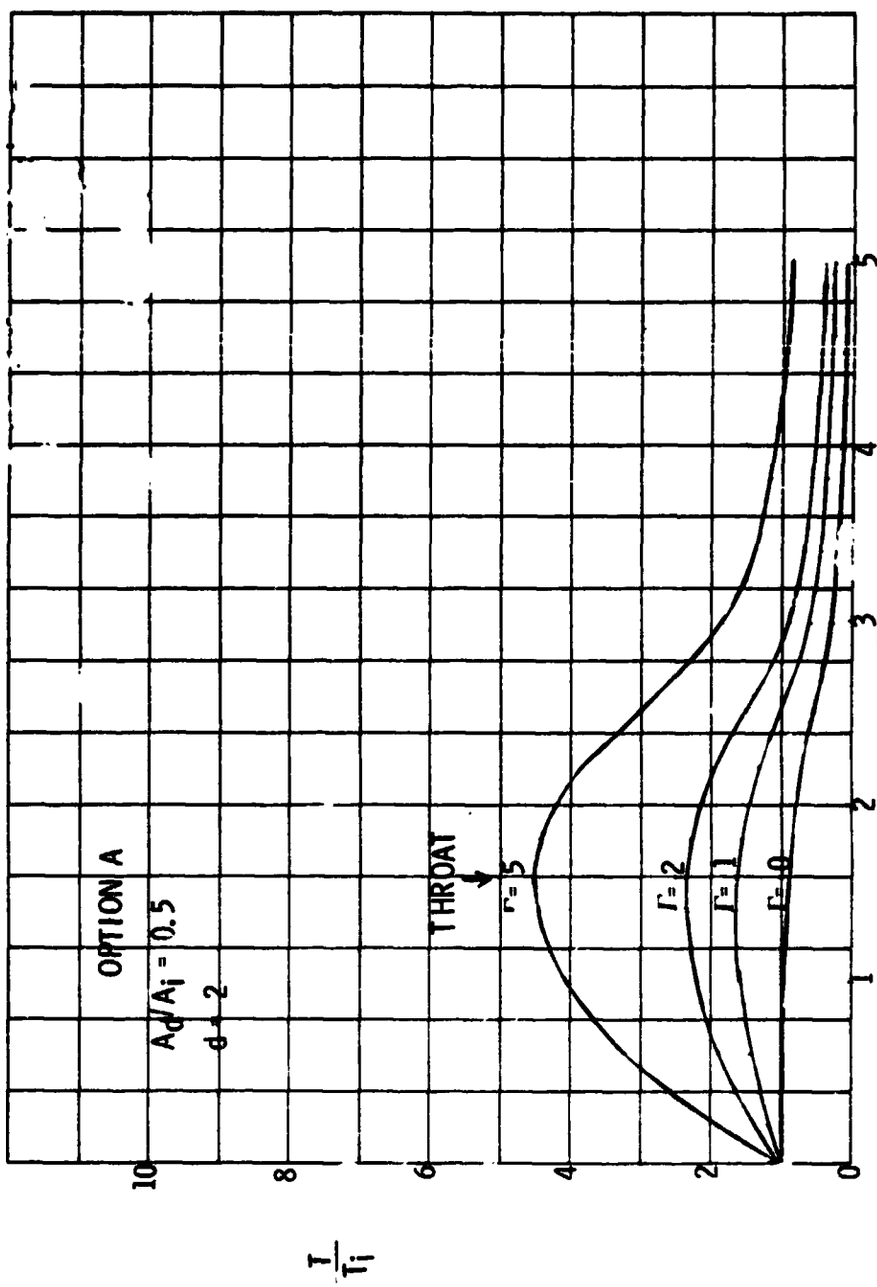

Fig. 5.7 Dimensionless temperature distribution

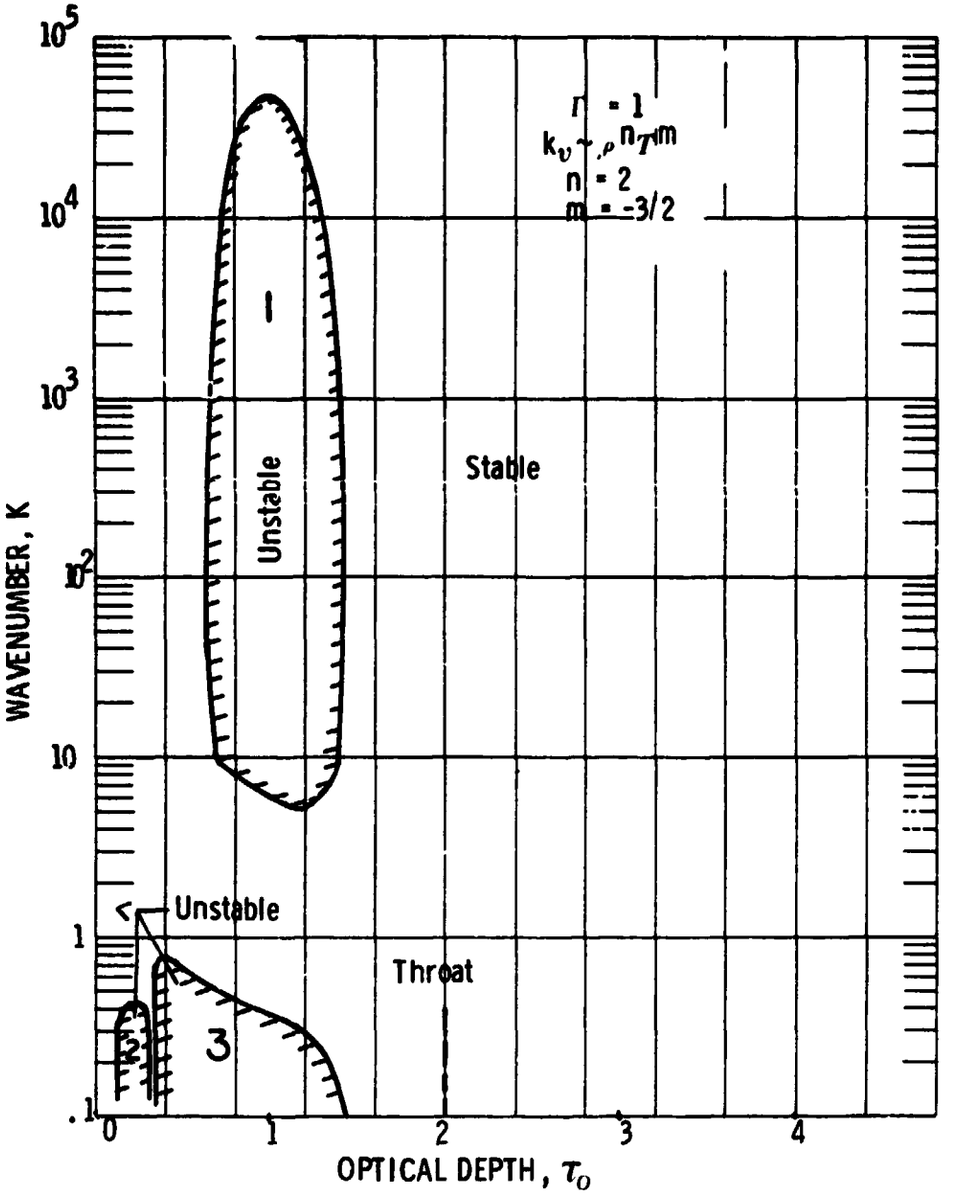

Fig. 5.8 Contours of neutral stability for Γ = 1

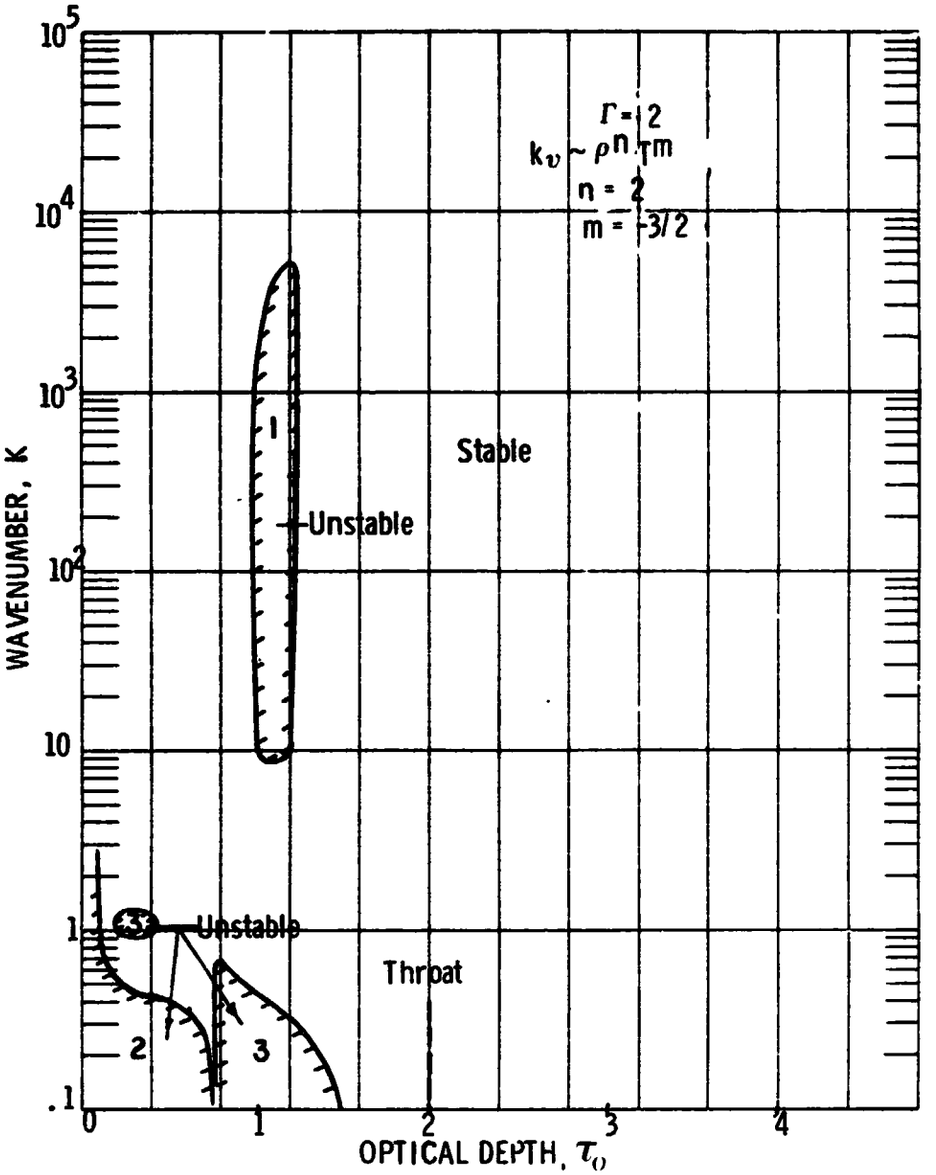

Fig. 5.9 Contours of neutral stability for $\Gamma = 2$

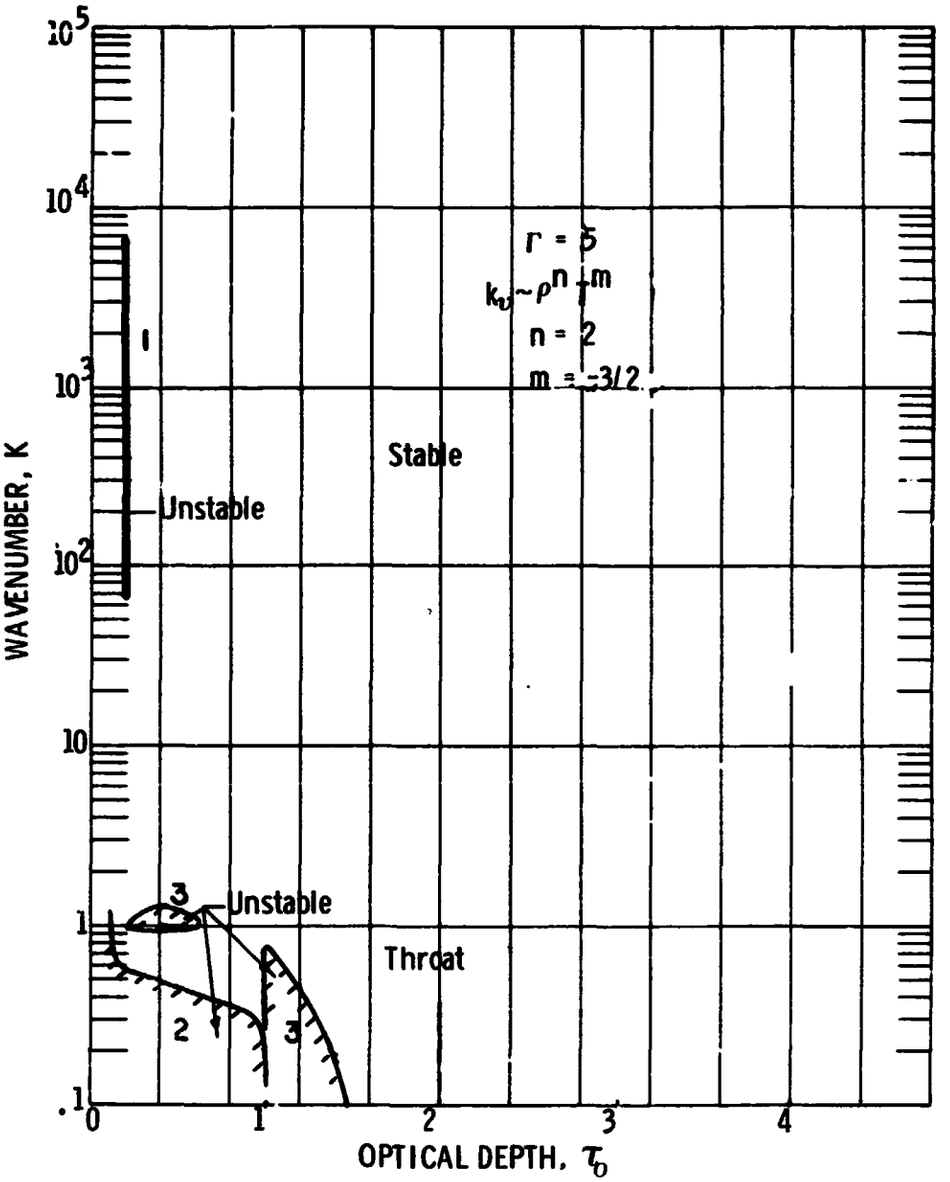

Fig. 5.10 Curves of neutral stability for $\Gamma = 5$

and grows in one region, will dampen after it travels to a new location. The analysis serves as an indicator as to where potential absorption wave phenomena may be initiated. It is desirable to design a nozzle/absorber arrangement which contains a minimum number and extent of these unstable zones.

The unstable zones are numbered 1, 2 or 3, corresponding to the three roots of Ω. Often at a specific location only one or two of these roots yields an unstable zone. For example, in Fig. 5.8 at $\tau_o = .3$ the second root results in the unstable region for $0.1 \leq K \leq .4$ and the first and third roots yield stable waves. At $\tau_o = 1$ the first and third roots result in unstable zones, but the second root yields stable waves. In addition, one root may yield several zones of instability. For example, in Fig. 5.9 the third root yields two distinct unstable zones, one at $.2 \leq \tau_o \leq .5$, $.9 \leq K \leq 1.1$ and the other at $.8 \leq \tau_o \leq 1.3$, $.1 \leq K \leq .8$. The unstable regions are upstream of the throat and near the inlet area as expected where the absorption takes place. It can be shown that the regions labeled 2 and 3 are physically unimportant by inverting Eq. (5.2) and returning to physical dimensions. This can be seen if we refer to Fig. 5.11.

Figure 5.11 presents the stability map translated into physical coordinates. x is the distance along the nozzle axis and most of the laser radiation is absorbed from x = 0 to x = 10 cm. For simplicity, the sample gas has been chosen to be helium with 0.1% of cesium to provide a fully ionized seed that absorbs by inverse Bremsstrahlung at the initial temperature $T_i = 5000^oK$. The initial pressure p_i is 5 atm and as stated the cesium concentration $Cs_c = 0.1\%$. The unstable zones are shaded and are located from x = 0 to x = 10 cm in the region where the absorption takes place. It is now necessary to determine which anticipated disturbance wave numbers are physically important. We must first determine an appropriate length scale to compare with the disturbance wavelength. The steady state solution for this example case indicates that by x = 10 cm most of the laser power has been absorbed. Therefore, a characteristic absorption length scale is 10 cm. If a disturbance has a wavelength much greater than 10 cm, the absorption will only affect a fraction of the wave and growth of the entire wave due to unstable heating will not be significant. Therefore, only disturbances of wavelengths less than 10 cm can be considered important. Since $K = 2\pi/\lambda$, where λ is the disturbance wave length, this implies that only wave number $K > 2\pi/10\ cm^{-1} \cong .6\ cm^{-1}$ are of interest. Unstable region #1 is the only important region. It is now desirable to make this region as small as possible to minimize the possibility of unstable heating in the nozzle. As the laser power is increased this unstable region decreases in size as is seen in Figs. 5.9 and 5.10. Therefore, a

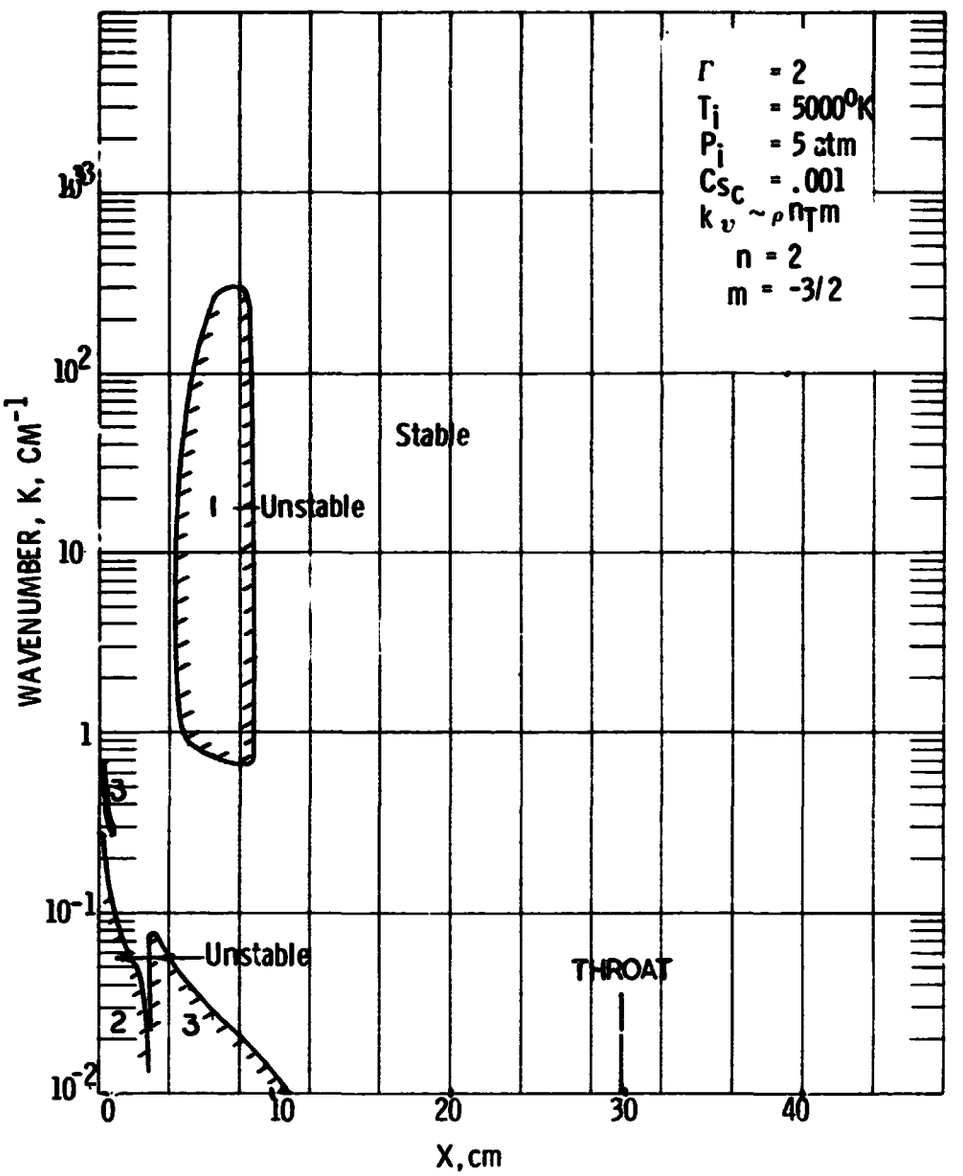

Fig. 5.11 Curves of neutral stability for Γ = 2 in physical dimensions

nozzle design based upon the conditions in Fig. 5.10 may be considered a good design for stable conversion of laser energy to kinetic energy.

5.5 SUMMARY

Analyses of the steady flow resulting from laser heating in a nozzle configuration and the resulting stability of such flows have been presented. It must be emphasized that the sample results of Figs. 5.1 - 5.11 are not necessarily for the most efficient nozzle design to convert laser power to high velocity exhaust. The analyses must be applied to other nozzle shapes and absorbers in order to optimize the power conversion efficiency.

REFERENCES

1. A. N. Pirri and R. F. Weiss, "Laser Propulsion," AIAA Paper No. 72-719, AIAA 5th Fluid and Plasma Dynamics Conference, Boston, Mass., June 1972.

2. A. N. Pirri, M. J. Monsler and P. E. Nebolsine, AIAA Journal, 12, 1254 (1974).

3. F. E. Rom and H. A. Putre, "Laser Propulsion," NASA TM-X-2510, April 1972.

4. A. Hertzberg, E. W. Johnston and H. G. Ahlstrom, "Photon Generators and Engines for Laser Power Transmission," AIAA Paper No. 71-105, AIAA 9th Aerospace Sciences Meeting, New York, N. Y., January 1971.

5. J. R. Stallcop, J. Plasma Phys. 11, 111 (1974)

6. J. R. Stallcop, Phys. Fluids 17, 751 (1974)

7. K. W. Billman, P. D. Rowley, J. R. Stallcop and L. Presley, Phys. Fluids 17, 759 (1974)

8. W. Finkelnburg, T. Peters, Handbuch d. Phys., Bd. 28, Springer Verlag, Berlin, 1957.

9. L. M. Biberman and G. E. Norman, Sov. Phys. Uspekhi, 10, 52 (1967)

10. R. R. Johnston, JQSRT 7, 815 (1967)

11. H. A. Kramers, Phil. Mag. 46, 836 (1923)

12. Y. B. Zeldovich and Y. P. Raizer, Physics of Shock Waves and High Temperature Hydrodynamic Phenomena, Vol. I. Academic Press, New York, 1966

13. J. A. Gaunt, Phil. Trans. R. Soc. London A 229, 163 (1930)

14. W. J. Karzas and R. Latter, Astrophys. J., Supplement Series 55, 167 (1961)

15. G. Peach, Mon. Not. Roy. Astron. Soc. 124, 371 (1975)

16. S. Geltman, JOSRT 13, 601 (1973)

17. O. B. Firsov and M. I. Chibisov, Sov. Phys. JETP, 12, 1235 (1961)

18. T. Ohmura and H. Ohmura, Astrophys. J. 131 8, (1960), also Phys. Rev. 121, 513 (1961)

19. T. L. John, Mon. Not. Royal Astron. Soc. 128, 93 (1964); 131, 315 (1966)

20. S. Geltman, Astrophys. J. 141, 376 (1965)

21. N. A. Doughty and P. A. Fraser, Mon. Not. Royal Astron. Soc. 132, 267 (1966)

22. J. L. Stilley and J. Callaway, Astrophys. J. 160, 245 (1970)

23. A. Dalgarno and N. Lane, Astrophys. J. 145, 623 (1966)

24. T. F. O'Malley, L. Spruch and L. Rosenberg, J. Math Phys. 2, 491 (1961)

25. J. R. Stallcop, Astrophys. J. 187, 179 (1974)

26. W. B. Somerville, Astrophysical J. 139, 192 (1964)

27. R. V. Devore, Phys. Rev. 136, A666 (1964); 140, AB3 (1965)

28. B. Kivel, JQSRT 7, 27 (1967); 7, 51 (1967)

29. R. C. Mjolsness and H. M. Ruppel, Phys. Rev. 154, 98 (1967)

30. T. L. John and A. R. Williams, J. Phys. B 5, 1662 (1972)

31. H. A. Hyman and B. Kivel, JQSRT 13, 699 (1973)

32. S. Geltman, private communication, 1974

33. V. M. Batchin and V. F. Chinnov, Sov. Phys. JETP 34, 30 (1972)

34. R. L. Taylor and G. Caledonia, JQSRT 9, 657 (1969)

35. R. T. V. Kung, unpublished results

36. R. L. Taylor and G. Caledonia, JQSRT 9, 681 (1969)

37. J. C. Morris, R. U. Krey and R. L. Garrison, Phys. Rev. 180, 167 (1969)

38. A. Konkov and A. V. Vorontsuv, Sov. Opt. Spectrosc. 33, 243 (1972)

39. R. W. Patch, JQSRT 9, 63 (1969)

40. H. A. Hyman and C. W. vonRosenberg, "Atomic Line Radiation in The Infrared," to be submitted

41. G. Herzberg, Molecular Spectra and Molecular Structure I. Spectra of Diatomic Molecules, D. Van Nostrand Co., New York, 1950

42. S. S. Penner, Quantitative Molecular Spectroscopy and Gas Emissivities, Addison-Wesley, Reading, Mass., 1959.

43. L. A. Young and W. J. Eachus, J. Chem. Phys. 44, 4195 (1966)

44. R. C. Millikan and D. R. White, J. Chem. Phys. 39, 3209 (1963)

45. C. W. vonRosenberg, Jr. and K. L. Wray, J. Chem. Phys. 54, 1406 (1971)

46. C. W. vonRosenberg, Jr., R. L. Taylor and J. D. Teare, J. Chem. Phys. 54, 1974 (1971)

47. R. E. Center, J. Chem. Phys. 58, 5230 (1973)

48. J. C. Stephenson, J. Chem. Phys. 60, 4289 (1974)

49. R. D. Bates, Jr., J. T. Knudtson, G. W. Flynn, Chem. Phys. letters 8, 103 (1971)

50. J. D. Anderson, Jr., AIAA J. 12, 1527

51. J. T. Knudtson and G. W. Flynn, J. Chem. Phys. 58, 1467 (1973)

52. W. D. Breshears and L. S. Blair, J. Chem. Phys. 59, 5824 (1973)

53. R. L. Taylor and S. Bitterman, Rev. Mod. Phys. 41, 26 (1969)

54. A. R. Strilchuck and A. A. Offenberger, App. Opt. 13, 2643 (1974)

55. H. C. Van deHulst Light Scattering by Small Particles, John Wiley and Sons, New York, 1957.

56. F. E. Volz, J. Geophys. Res. 77, 1017 (1972)

57. T. R. Steyer, K. L. Day, D. R. Huffman, App. Opt. 13, 1586 (1974)

58. C. D. Lanzo, J. Opt. Soc. Amer. 58, 1630 (1968)

59. H. S. Carslaw and J. C. Jaeger, "Conduction of Heat in Solids", Oxford at the Clarendon Press, 1959

60. W. G. Vincenti and S. C. Traugott, "The Coupling of Radiative Transfer and Gas Motion", Annual Review of Fluid Mechanics, Vol. 3, 1971, pp. 89-117

61. M. J. Monsler, "An Acoustic Instability Driven by Absorption of Radiation in Gases". PhD thesis, M.I.T., Cambridge, Mass. 1969.

62. W. G. Vincenti and C. H. Kruger, Jr., Introduction to Physical Gas Dynamics, Wiley, New York (1965), pp. 463.

63. A. H. Shapiro, Compressible Fluid Flow, The Ronald Press Co., New York, Vol. I (1953).

64. V. R. Buonadonna, C. R. Knight, and A. Hertzberg, AIAA J. 11, 11, 1457-58, Nov. 1973.